Supporting Information

Synthesis and characterization of 0D - 3D copper-containing tungstobismuthates obtained from the lacunary precursor $Na_9[B\text{-}\alpha\text{-}BiW_9O_{33}]$

Kim D. von Allmen, Henrik Grundmann, Anthony Linden, and Greta R. Patzke*

Department of Chemistry

University of Zurich

Winterthurerstrasse 190, CH-8057 Zurich, Switzerland

Contents

1 Literature survey

Table S1. Reported Cu substituted tungstobismuthates prepared from the $[B\text{-}\alpha\text{-}BiW_9O_{33}]^{9-}$ precursor.

Polyoxometalate	Main structural motif	Ref.
$[Cu_3(H_2O)_3(B\text{-}\alpha\text{-}XW_9O_{33})_2]^{n-}$ (X = As, Sb, Se, Te; n = 10 for Te and Se, 12 for Sb, As)	$Cu_3(H_2O)_3O_3$	1
$Na_{12}[Cu_3(H_2O)_3(B\text{-}\alpha\text{-}BiW_9O_{33})_2]\cdot 47H_2O$	$Cu_3(H_2O)_3O_3$	2
$Na_{12}[Cu_3(H_2O)_3(B\text{-}\alpha\text{-}BiW_9O_{33})_2]$	$Cu_3(H_2O)_3O_3$	4
$Na_{12}[Cu_3(H_2O)_3(B\text{-}\alpha\text{-}BiW_9O_{33})_2]\cdot 29H_2O$	$Cu_3(H_2O)_3O_3$	5
$2D\text{-}Na_5(TEOA\text{-}H)_4[(Cu(H_2O))_3(B\text{-}\alpha\text{-}BiW_9O_{33})_2]$	$Cu_3(H_2O)_3O_3$	3
$Na_{10}[Cu_4(H_2O)_2(B\text{-}\alpha\text{-}BiW_9O_{33})_2]\cdot 43H_2O$	$Cu_4(H_2O)_2$	5
$Na_{12}[\{Cu(H_2O)_2\}_3(B\text{-}\alpha\text{-}BiW_9O_{33})_2]\cdot 42H_2O$	$Cu_3(H_2O)_3O_3$	6
$2D\text{-}[enH_2]_5[Cu^{II}(en)_2][Cu^{I}_2(WO_2)_2(B\text{-}\beta\text{-}SbW_9O_{33})_2]\cdot 16H_2O$	$Cu_2(H_2O)_2W_2O_4$	3
$2D\text{-}[enH_2]_5[Cu^{II}(en)_2][Cu^{I}_2(WO_2)_2(B\text{-}\beta\text{-}BiW_9O_{33})_2]\cdot 22H_2O$	$Cu_2(H_2O)_2W_2O_4$	3
$Na_8[Bi_2W_{20}Cu_2O_{68}(OH)_2(H_2O)_6]\cdot 26H_2O$	$Cu_2(H_2O)_2W_2O_4$	5
$Na_6H_4[Bi_2Cu_2W_{20}O_{70}(H_2O)_6]\cdot 36H_2O$	$Cu_2(H_2O)_2W_2O_4$	7
$KNa_3[Cu(H_2O)_2\{Cu(H_2O)_3\}_2(H_2W_{12}O_{42})]\cdot 16H_2O$	$W_{12}O_{42}\text{-}M_x$	8
$\{Cu(H_2O)_4\}_2\{Cu_2(\mu\text{-}OH)_2(H_2O)_6\}(H_2W_{12}O_{42})]\cdot 10H_2O$	$W_{12}O_{42}\text{-}M_x$	9
$(NH_4)_8[Cu(H_2O)_2H_2W_{12}O_{42}]\cdot 10H_2O$	$W_{12}O_{42}\text{-}M_x$	10
$Na_8[Cu(H_2O)_2(H_2W_{12}O_{42})]\cdot 30H_2O$	$W_{12}O_{42}\text{-}M_x$	11
$3D\text{-}[Cu(H_2O)_6][\{Cu(H_2O)_2\}_2\{Cu(H_2O)_4H_4W_{12}O_{42}\}]\cdot 12H_2O$	$W_{12}O_{42}\text{-}M_x$	12
$1D\text{-}[Na_2(H_2O)_8][Na_8(H_2O)_{20}][Cu(en)_2][W_{12}O_{42}]\cdot 3H_2O$	$W_{12}O_{42}\text{-}M_x$	13
$Na_2Cu_3(CuOH)[W_{12}O_{40}(OH)_2]\cdot 32H_2O$	$W_{12}O_{42}\text{-}M_x$	14
$Na_{12}[(Na(H_2O)_2)_6(B\text{-}\alpha\text{-}BiW_9O_{33})_2]$	Various	15
$[H_2bipy][Cu(bipy)(H_2O)_2][Cu(bipy)_3][H_3BiW_{18}O_{60}]\cdot H_2O$		16

2 Crystallographic and structural characterization

Single-crystals were selected and mounted on a glass fiber loop with Infineum oil. The crystal was placed in a dry N_2 gas stream and X-ray diffraction intensity data were collected at 183 K, on an Oxford Xcalibur Ruby CCD single crystal diffractometer equipped with an Enhance Mo X-ray source (Mo K_α radiation, λ = 0.7107 Å) and a graphite monochromator. An Oxford Instruments Cryojet system was used for cooling the crystal. All data processing and a numerical absorption correction were carried out using CrysAlisPro, Version 1.171.36.32, Agilent (2014). The WinGX software package was employed for structure solution and refinement. An initial structure solution was obtained from SHELXT (2014/4),[17] and refined with SHELXL (2014/7).[17] For structure validation, PLATON was used.[18] CIF files were modified and checked for errors with EnCIFer 1.5.[19] Hydrogen atoms could not be located from the difference Fourier maps and were therefore not refined. Low angle reflections, attenuated by the beamstop, were omitted, as well as reflections above 55°. After subsequent assignment of residual electron density with partially occupied crystal water molecules, no more voids were observed. Residual electron density below 1 $e^{-}Å^{-3}$ was generally considered as noise. For the structurally related compounds **Cu-1**, **Cu-2** and **Cu-3**, an identical labelling scheme for W atoms was used. Rigid bond restraints (RIGU) have been applied in all refinements.

The three highest remaining electron density peaks in the structure **Cu-3** were located between 4.23 and 5.96 $e^{-}Å^{-3}$, at distances from W atoms of less than 1.0 Å. Despite several attempts to perform an analytical and Gaussian absorption correction, the sizes of these peaks could not be diminished. For the structures **Cu-1**, **Cu-2**, and **Cu-4** – **Cu-6** the highest remaining electron density peaks were between 1.3 and 3.0 $e^{-} A^{-3}$.
This is in agreement with residual electron density peaks found for other reported polyoxometalate structures with characteristic values of 2.35-4.34 $e^{-} A^{-3}$.[20–22]

Details on the crystal structures as well as the crystallographic information files (CIF) may be obtained from the Fachinformationszentrum Karlsruhe, D-76344 Eggenstein-Leopoldshafen, Germany (Fax: +49 7247 808 666; email crysdata@fiz-karlsruhe.de), by citing the depository numbers CSD-431217 (**Cu-1**), CSD-431215 (**Cu-2**), CSD-431213 (**Cu-3**), CSD-431218 (**Cu-4**), CSD-431216 **(Cu-5)**, and CSD-431214 **(Cu-6)**.

Table S2. Summary of the crystal structure refinements for **Cu-1** – **Cu-6.**

	Cu-1	**Cu-2**	**Cu-3**	**Cu-4**	**Cu-5**	**Cu-6**
Empirical formula	$Bi_2ClCu_2H_{83}Na_{11}O_{11.5}W_{20}$	$Bi_2Cu_{2.5}H_{66}K_3Na_7O_{103.5}W_{20}$	$Bi_2Cu_3H_{43}K_{2.5}Na_{5.5}O_{91.5}W_{20}$	$Bi_2Cu_3H_{48}Na_6O_{91}Rb_6W_{18}$	$Bi_2ClCu_{3.82}H_{15.93}K_{9.18}O_{82}W_{18}$	$CuH_{26}K_4Na_4O_{66}W_{12}$
Formula weight (g mol^{-1})	6378.04	6289.80	6016.84	6072.76	5692.17	3600.12
Temperature (K)	183	183	183	183	183	183
Wavelength (λ/Å)	0.71073	0.71073	0.71073	0.71073	0.71073	0.71073
Crystal system	Triclinic	Triclinic	Triclinic	Monoclinic	Tetragonal	Monoclinic
Space group	*P*-1	*P*-1	*P*-1	$P2_1/m$	$P\bar{4}2_1m$	$P2_1/n$
a (Å)	13.0484(2)	12.1737(3)	11.5922(3)	13.2273(7)	16.6507(3)	13.1440(3)
b (Å)	17.4970(4)	18.8865(5)	17.4118(5)	19.3688(5)	16.6610(3)	11.5894(2)
c (Å)	23.2335(4)	22.3984(5)	20.5750(6)	18.1322(5)	13.7954(2)	19.0984(5)
α (°)	80.2569(17)	93.782(2)	95.335(2)	90	89.9885(13)	90
β (°)	89.1164(14)	95.696(2)	93.951(2)	98.083(3)	89.9890(12)	103.752(2)
γ (°)	71.4112(17)	99.016(2)	105.546(3)	90	89.9652(13)	90
V ($Å^3$)	4950.93(16)	5043.6(2)	3964.5(2)	4599.3(3)	3827.08(10)	2825.88(11)
Z	2	2	2	2	2	2
F(000)	5634	5493	5232	4966	4944	3258
M (mm-1)	27.289	26.987	34.374	30.187	33.192	25.138
ρ_{calc} (g/cm^{-3})	4.278	4.142	5.041	4.385	4.940	4.230
Crystal size (mm)	0.22 x 0.10 x 0.06	0.30 x 0.16 x 0.06	0.26 x 0.12 x 0.04	0.28 x 0.10 x 0.07	0.20 x 0.11 x 0.05	0.20 x 0.12 x 0.05
Reflections collected/unique	98674/22727	53429/23139	38976/18204	43254/10866	31680/4603	28159/6481
Unique observed reflections	18994	18536	13677	8254	4424	6002
θ range (°)	2.57-32.90	2.444-27.500	2.445-27.500	2.9090-30.5550	2.466-27.499	2.770-27.497
Data/restraints/parameters	22727/2295/1396	23139/2280/1420	18204/2076/1159	10866/1491/670	4603/774/342	6481/519/394
Goodness-of-fit	1.059	1.062	1.031	1.030	0.927	1.047
R_1[a] [I>2σ(I)]	0.0325	0.0410	0.0460	0.0610	0.0224	0.0236
wR_2[b] (all data)	0.0745	0.1058	0.1091	0.1712	0.0622	0.0641

[a] = R(F) [I > 2σ(I) reflections] ; [b] = wR(F^2) (all data)

Table S3. List of selected bond lengths for **Cu-1a** (left) and **Cu-1b** (right; ax. = axial, ter. = terminal, eq. = equatorial)

Cu-1a

Bond	d / Å	Bond	d / Å	Bond	d / Å
W(1A)-O(8A)$_{ax.}$	2.198(6)	W(4A)-O(1A)$_{ax.}$	2.250(6)	W(7A)-O(23A)$_{ax.}$	2.241(6)
W(1A)-O(17A)$_{ter.}$	1.732(6)	W(4A)-O(34A)$_{ter.}$	1.715(6)	W(7A)-O(30A)$_{ter.}$	1.717(6)
W(1A)-O(35A)$_{eq.}$	1.807(6)	W(4A)-O(31A)$_{eq.}$	1.944(6)	W(7A)-O(18A)$_{eq.}$	2.001(6)
W(1A)-O(32A)$_{eq.}$	1.814(6)	W(4A)-O(3A)$_{eq.}$	1.900(6)	W(7A)-O(19A)$_{eq.}$	2.024(7)
W(1A)-O(16A)$_{eq.}$	2.093(6)	W(4A)-O(10A)$_{eq.}$	1.898(7)	W(7A)-O(14A)$_{eq.}$	1.906(6)
W(1A)-O(9A)$_{eq.}$	2.024(6)	W(4A)-O(15A)$_{eq.}$	1.955(6)	W(7A)-O(22A)$_{eq.}$	1.799(7)
W(2A)-O(8A)$_{ax.}$	2.306(6)	W(5A)-O(1A)$_{ax.}$	2.228(6)	W(8A)-O(23A)$_{ax.}$	2.229(6)
W(2A)-O(26A)$_{ter.}$	1.714(7)	W(5A)-O(33A)$_{ter.}$	1.732(6)	W(8A)-O(25A)$_{ter.}$	1.740(6)
W(2A)-O(15A)$_{eq.}$	1.872(7)	W(5A)-O(3A)$_{eq.}$	2.016(6)	W(8A)-O(4A)$_{eq.}$	1.885(6)
W(2A)-O(13A)$_{eq.}$	2.026(6)	W(5A)-O(5A)$_{eq.}$	1.822(7)	W(8A)-O(6A)$_{eq.}$	1.947(6)
W(2A)-O(7A)$_{eq.}$	1.944(6)	W(5A)-O(14A)$_{eq.}$	1.917(6)	W(8A)-O(12A)$_{eq.}$	1.932(7)
W(2A)-O(16A)$_{eq.}$	1.837(6)	W(5A)-O(24A)$_{eq.}$	1.970(7)	W(8A)-O(18A)$_{eq.}$	1.910(6)
W(3A)-O(8A)$_{ax.}$	2.296(6)	W(6A)-O(1A)$_{ax.}$	2.196(6)	W(9A)-O(23A)$_{ax.}$	2.260(7)
W(3A)-O(29A)$_{ter.}$	1.716(7)	W(6A)-O(28A)$_{ter.}$	1.725(7)	W(9A)-O(21A)$_{ter.}$	1.711(7)
W(3A)-O(20A)$_{eq.}$	1.954(6)	W(6A)-O(10A)$_{eq.}$	2.010(6)	W(9A)-O(2A)$_{eq.}$	1.946(6)
W(3A)-O(6A)$_{eq.}$	1.894(6)	W(6A)-O(24A)$_{eq.}$	1.956(6)	W(9A)-O(20A)$_{eq.}$	1.894(6)
W(3A)-O(9A)$_{eq.}$	1.881(6)	W(6A)-O(2A)$_{eq.}$	1.869(6)	W(9A)-O(12A)$_{eq.}$	1.923(6)
W(3A)-O(7A)$_{eq.}$	1.931(6)	W(6A)-O(13A)$_{eq.}$	1.860(6)	W(9A)-O(19A)$_{eq.}$	1.904(6)
W(10A)-O(11A)$_{ter.}$	1.735(7)	Cu(1A)-O(17A)$_{ap.}$	2.195(6)	BI(1A)-O(8A)	2.144(6)
W(10A)-O(27A)$_{ter.}$	1.742(6)	Cu(1A)-O(36A)$_{ap.}$	2.9241(1)	BI(1A)-O(23A)	2.150(6)
W(10A)-O(31A)	1.949(6)	Cu(1A)-Cl(1A)	2.280(3)	BI(1A)-O(1A)	2.150(6)
W(10A)-O(4A)	2.004(6)	Cu(1A)-O(37A)	1.964(6)		
W(10A)-O(32A)	2.129(6)	Cu(1A)-O(22A)	1.929(7)		
W(10A)-O(35A)	2.121(6)	Cu(1A)-O(5A)	1.956(6)		

Cu-1b

Bond	d / Å	Bond	d / Å	Bond	d / Å
W(1B)-O(30B)$_{ax.}$	2.190(6)	W(4B)-O(11B)$_{ax.}$	2.248(6)	W(7B)-O(19B)$_{ax.}$	2.216(6)
W(1B)-O(18B)$_{ter.}$	1.731(6)	W(4B)-O(26B)$_{ter.}$	1.717(6)	W(7B)-O(28B)$_{ter.}$	1.732(6)
W(1B)-O(12B)$_{eq.}$	1.803(7)	W(4B)-O(9B)$_{eq.}$	1.880(7)	W(7B)-O(1B)$_{eq.}$	1.971(6)
W(1B)-O(17B)$_{eq.}$	2.052(6)	W(4B)-O(29B)$_{eq.}$	1.892(6)	W(7B)-O(4B)$_{eq.}$	1.960(6)
W(1B)-O(20B)$_{eq.}$	2.069(7)	W(4B)-O(2B)$_{eq.}$	1.937(7)	W(7B)-O(23B)$_{eq.}$	1.944(6)
W(1B)-O(8B)$_{eq.}$	1.811(6)	W(4B)-O(16B)$_{eq.}$	1.956(6)	W(7B)-O(10B)$_{eq.}$	1.817(7)
W(2B)-O(30B)$_{ax.}$	2.298(6)	W(5B)-O(11B)$_{ax.}$	2.206(6)	W(8B)-O(19B)$_{ax.}$	2.252(6)
W(2B)-O(24B)$_{ter.}$	1.713(7)	W(5B)-O(35B)$_{ter.}$	1.735(6)	W(8B)-O(22B)$_{ter.}$	1.727(6)
W(2B)-O(13B)$_{eq.}$	1.921(6)	W(5B)-O(3B)$_{eq.}$	1.787(7)	W(8B)-O(14B)$_{eq.}$	1.930(6)
W(2B)-O(20B)$_{eq.}$	1.873(7)	W(5B)-O(4B)$_{eq.}$	1.889(6)	W(8B)-O(5B)$_{eq.}$	1.876(7)
W(2B)-O(16B)$_{eq.}$	1.892(6)	W(5B)-O(6B)$_{eq.}$	2.013(7)	W(8B)-O(1B)$_{eq.}$	1.926(6)
W(2B)-O(25B)$_{eq.}$	1.972(6)	W(5B)-O(29B)$_{eq.}$	2.018(6)	W(8B)-O(7B)$_{eq.}$	1.944(7)
W(3B)-O(30B)$_{ax.}$	2.306(6)	W(6B)-O(11B)$_{ax.}$	2.283(7)	W(9B)-O(19B)$_{ax.}$	2.220(6)
W(3B)O(27B)$_{ter.}$	1.721(6)	W(6B)-O(32B)$_{ter.}$	1.713(7)	W(9B)-O(33B)$_{ter.}$	1.732(7)
W(3B)-O(13B)$_{eq.}$	1.937(7)	W(6B)-O(2B)$_{eq.}$	1.917(6)	W(9B)-O(15B)$_{eq.}$	1.884(6)
W(3B)-O(21B)$_{eq.}$	1.988(6)	W(6B)-O(6B)$_{eq.}$	1.913(6)	W(9B)-O(23B)$_{eq.}$	1.961(6)
W(3B)-O(14B)$_{eq.}$	1.886(7)	W(6B)-O(15B)$_{eq.}$	1.947(6)	W(9B)-O(21B)$_{eq.}$	1.846(6)
W(3B)-O(17B)$_{eq.}$	1.853(7)	W(6B)-O(25B)$_{eq.}$	1.889(6)	W(9B)-O(5B)$_{eq.}$	2.015(6)
W(10B)-O(31B)$_{ter.}$	1.736(7)	Cu(1B)-O(38B)$_{ap.}$	2.9303(1)	Bi(1B)-O(30B)	2.146(6)
W(10B)-O(34B)$_{ter.}$	1.755(6)	Cu(1B)-O(18B)$_{ap.}$	2.216(7)	Bi(1B)-O(11B)	2.157(6)
W(10B)-O(7B)	1.940(7)	Cu(1B)-O(37B)	1.973(6)	Bi(1B)-O(19B)	2.135(6)
W(10B)-O(8B)	2.098(6)	Cu(1B)-O(36B)	1.982(7)		
W(10B)-O(9B)	2.006(6)	Cu(1B)-O(10B)	1.934(6)		
W(10B)-O(12B)	2.152(7)	Cu(1B)-O(3B)	1.957(6)		

Table S4. List of selected bond lengths for **Cu-2** (ax. = axial, ter. = terminal, eq. = equatorial).

Cu-2a

Bond	d / Å	Bond	d / Å	Bond	d / Å
W(1A)-O(6A)$_{ax.}$	2.197(9)	W(4A)-O(18A)$_{ax.}$	2.244(9)	W(7A)-O(4A)$_{ax.}$	2.227(9)
W(1A)-O(28A)$_{ter.}$	1.733(9)	W(4A)-O(23A)$_{ter.}$	1.703(9)	W(7A)-O(17A)$_{ter}$	1.736(10)
W(1A)-O(1A)$_{eq.}$	2.069(9)	W(4A)-O(25A)$_{eq.}$	1.883(9)	W(7A)-O(10A)$_{eq.}$	1.959(9)
W(1A)-O(2A)$_{eq.}$	2.035(10)	W(4A)-O(8A)$_{eq.}$	1.964(9)	W(7A)-O(15A)$_{eq.}$	1.959(8)
W(1A)-O(19A)$_{eq.}$	1.823(8)	W(4A)-O(13A)$_{eq.}$	1.916(9)	W(7A)-O(20A)$_{eq.}$	1.801(9)
W(1A)-O(11A)$_{eq.}$	1.819(9)	W(4A)-O(29A)$_{eq.}$	1.924(9)	W(7A)-O(27A)$_{eq.}$	2.029(9)
W(2A)-O(6A)$_{ax.}$	2.288(9)	W(5A)-O(18A)$_{ax.}$	2.207(9)	W(8A)-O(4A)$_{ax.}$	2.266(8)
W(2A)-O(24A)$_{ter.}$	1.708(10)	W(5A)-O(14A)$_{ter.}$	1.716(9)	W(8A)-O(16A)$_{ter.}$	1.707(10)
W(2A)-O(2A)$_{eq.}$	1.872(9)	W(5A)-O(7A)$_{eq.}$	1.784(10)	W(8A)-O(15A)$_{eq.}$	1.906(9)
W(2A)-O(30A)$_{eq.}$	1.932(9)	W(5A)-O(10A)$_{eq.}$	1.922(9)	W(8A)-O(35A)$_{eq.}$	1.927(9)
W(2A)-O(26A)$_{eq.}$	1.971(9)	W(5A)-O(13A)$_{eq.}$	1.988(9)	W(8A)-O(12A)$_{eq.}$	1.939(10)
W(2A)-O(8A)$_{eq.}$	1.885(9)	W(5A)-O(22A)$_{eq.}$	2.013(10)	W(8A)-O(32A)$_{eq.}$	1.910(10)
W(3A)-O(6A)$_{ax.}$	2.328(9)	W(6A)-O(18A)$_{ax.}$	2.290(9)	W(9A)-O(4A)$_{ax.}$	2.255(8)
W(3A)-O(3A)$_{ter.}$	1.720(9)	W(6A)-O(31A)$_{ter.}$	1.750(10)	W(9A)-O(33A)$_{ter.}$	1.718(9)
W(3A)-O(1A)$_{eq.}$	1.854(9)	W(6A)-O(5A)$_{eq.}$	1.915(9)	W(9A)-O(5A)$_{eq.}$	1.878(9)
W(3A)-O(30A)$_{eq.}$	1.937(10)	W(6A)-O(22A)$_{eq.}$	1.903(10)	W(9A)-O(27A)$_{eq.}$	1.884(10)
W(3A)-O(21A)$_{eq.}$	1.976(9)	W(6A)-O(29A)$_{eq.}$	1.976(9)	W(9A)-O(32A)$_{eq.}$	1.984(10)
W(3A)-O(12A)$_{eq.}$	1.878(10)	W(6A)-O(26A)$_{eq.}$	1.875(9)	W(9A)-O(21A)$_{eq.}$	1.891(9)
W(10A)-O(9A)$_{ter.}$	1.741(10)	Cu(1A)-O(27B)$_{ap.}$	2.5525(1)	Bi(1A)-O(18A)	2.134(8)
W(10A)-O(34A)$_{ter.}$	1.762(8)	Cu(1A)-O(28A)$_{ap.}$	2.302(9)	Bi(1A)-O(4A)	2.137(8)
W(10A)-O(11A)$_{eq.}$	2.122(9)	Cu(1A)-O(36A)	1.984(10)	Bi(1A)-O(6A)	2.129(9)
W(10A)-O(19A)$_{eq.}$	2.119(8)	Cu(1A)-O(37A)	1.966(12)		
W(10A)-O(25A)$_{eq.}$	1.995(8)	Cu(1A)-O(7A)	1.976(10)		
W(10A)-O(35A)$_{eq.}$	1.949(9)	Cu(1A)-O(20A)	1.939(8)		

Cu-2b

Bond	d / Å	Bond	d / Å	Bond	d / Å
W(1B)-O(13B)$_{ax.}$	2.197(8)	W(4B)-O(12B)$_{ax.}$	2.243(8)	W(7B)-O(1B)$_{ax.}$	2.257(8)
W(1B)-O(25B)$_{ter.}$	1.746(8)	W(4B)-O(21B)$_{ter.}$	2.337(8)	W(7B)-O(27B)$_{ter.}$	1.715(9)
W(1B)-O(6B)$_{eq.}$	2.040(9)	W(4B)-O(15B)$_{eq.}$	1.881(9)	W(7B)-O(2B)$_{eq.}$	1.967(8)
W(1B)-O(8B)$_{eq.}$	2.081(8)	W(4B)-O(20B)$_{eq.}$	1.937(9)	W(7B)-O(5B)$_{eq.}$	1.990(9)
W(1B)-O(32B)$_{eq.}$	1.809(8)	W(4B)-O(23B)$_{eq.}$	1.998(8)	W(7B)-O(16B)$_{eq.}$	1.967(8)
W(1B)-O(33B)$_{eq.}$	1.815(9)	W(4B)-O(31B)$_{eq.}$	1.904(9)	W(7B)-O(19B)$_{eq.}$	1.814(9)
W(2B)-O(13B)$_{ax.}$	2.300(8)	W(5B)-O(12B$_{)ax.}$	2.218(8)	W(8B)-O(1B)$_{ax.}$	2.243(8)
W(2B)-O(26B)$_{ter.}$	1.709(9)	W(5B)-O(17B)$_{ter.}$	1.729(8)	W(8B)-O(35B)$_{ter.}$	1.716(9)
W(2B)-O(23B)$_{eq.}$	1.842(8)	W(5B)-O(11B)$_{eq.}$	1.998(9)	W(8B)-O(2B)$_{eq.}$	1.918(8)
W(2B)-O(6B)$_{eq.}$	1.870(8)	W(5B)-O(15B)$_{eq.}$	2.038(8)	W(8B)-O(3B)$_{eq.}$	1.925(8)
W(2B)-O(10B)$_{eq.}$	1.955(8)	W(5B)-O(16B)$_{eq.}$	1.876(9)	W(8B)-O(4B)$_{eq.}$	1.922(9)
W(2B)-O(24B)$_{eq.}$	1.983(9)	W(5B)-O(18B)$_{eq.}$	1.822(9)	W(8B)-O(7B)$_{eq.}$	1.924(8)
W(3B)-O(13B)$_{ax.}$	2.337(8)	W(6B)-O(12B)$_{ax.}$	2.276(9)	W(9B)-O(1B)$_{ax.}$	2.251(8)
W(3B)-O(22B)$_{ter.}$	1.730(8)	W(6B)-O(34B)$_{ter.}$	1.731(10)	W(9B)-O(29B$_{)ter.}$	1.727(9)
W(3B)-O(3B)$_{eq.}$	1.901(9)	W(6B)-O(9B)$_{eq.}$	1.900(9)	W(9B)-O(4B)$_{eq.}$	1.992(8)
W(3B)-O(8B)$_{eq.}$	1.859(9)	W(6B)-O(11B)$_{eq.}$	1.908(9)	W(9B)-O(5B)$_{eq.}$	1.923(8)
W(3B)-O(10B)$_{eq.}$	1.931(9)	W(6B)-O(20B)$_{eq.}$	1.973(9)	W(9B)-O(9B)$_{eq.}$	1.901(8)
W(3B)-O(14B)$_{eq.}$	1.993(8)	W(6B)-O(24B)$_{eq.}$	1.874(9)	W(9B)-O(14B)$_{eq.}$	1.861(9)
W(10B)-O(30B)$_{ter.}$	1.752(9)	Cu(1B)-O(17A)$_{ap.}$	2.846(11)	Bi(1B)-O(1B)	2.128(8)
W(10B)-O(28B)$_{ter.}$	1.737(9)	Cu(1B)-O(25B)$_{ap.}$	2.191(8)	Bi(1B)-O(12B)	2.141(9)
W(10B)-O(7B)	1.971(8)	Cu(1B)-O(18B)	1.934(9)	Bi(1B)-O(13B)	2.117(8)
W(10B)-O(31B)	1.971(8)	Cu(1B)-O(19B)	1.931(8)		
W(10B)-O(32B)	2.131(8)	Cu(1B)-O(36B)	1.991(9)		
W(10B)-O(33B)	2.108(9)	Cu(1B)-O(37B)	2.001(9)		

Table S5. List of selected bond lengths for **Cu-3** (ax. = axial, ter = terminal, eq. = equatorial).

Cu-3a

Bond	d / Å	Bond	d / Å	Bond	d / Å
W(1A)-O(28A)$_{ax.}$	2.229(11)	W(4A)-O(18A)$_{ax.}$	2.231(11)	W(7A)-O(37A)$_{ax.}$	2.217(11)
W(1A)-O(10A)$_{ter.}$	1.749(12)	W(4A)-O(34A)$_{ter.}$	1.725(11)	W(7A)-O(17A)$_{ter.}$	1.748(11)
W(1A)-O(1A)$_{eq.}$	1.807(11)	W(4A)-O(2A)$_{eq.}$	1.917(11)	W(7A)-O(5A)$_{eq.}$	1.958(11)
W(1A)-O(21A)$_{eq.}$	1.807(11)	W(4A)-O(9A)$_{eq.}$	1.902(12)	W(7A)-O(6A)$_{eq.}$	1.936(11)
W(1A)-O(14A)$_{eq.}$	2.064(11)	W(4A)-O(25A)$_{eq.}$	1.895(11)	W(7A)-O(7A)$_{eq.}$	1.936(11)
W(1A)-O(19A)$_{eq.}$	2.040(12)	W(4A)-O(22A)$_{eq.}$	1.992(12)	W(7A)-O(13A)$_{eq.}$	1.794(11)
W(2A)-O(28A)$_{ax.}$	2.271(11)	W(5A)-O(18A)$_{ax.}$	2.222(12)	W(8A)-O(37A)$_{ax.}$	2.218(10)
W(2A)-O(35A)$_{ter.}$	1.765(13)	W(5A)-O(33A)$_{ter.}$	1.729(12)	W(8A)-O(29A)$_{ter.}$	1.711(11)
W(2A)-O(15A)$_{eq.}$	1.925(12)	W(5A)-O(4A)$_{eq.}$	1.790(11)	W(8A)-O(3A)$_{eq.}$	1.922(12)
W(2A)-O(16A)$_{eq.}$	1.978(12)	W(5A)-O(6A)$_{eq.}$	1.942(11)	W(8A)-O(5A)$_{eq.}$	1.952(12)
W(2A)-O(14A)$_{eq.}$	1.868(12)	W(5A)-O(11A)$_{eq.}$	2.014(12)	W(8A)-O(8A)$_{eq.}$	1.937(12)
W(2A)-O(22A)$_{eq.}$	1.850(12)	W(5A)-O(9A)$_{eq.}$	1.968(11)	W(8A)-O(20A)$_{eq.}$	1.899(11)
W(3A)-O(28A)$_{ax.}$	2.299(11)	W(6A)-O(18A)$_{ax.}$	2.260(12)	W(9A)-O(37A)$_{ax.}$	2.284(11)
W(3A)-O(26A)$_{ter.}$	1.746(12)	W(6A)-O(32A)$_{ter.}$	1.695(13)	W(9A)-O(36A)$_{ter.}$	1.736(12)
W(3A)-O(3A)$_{eq.}$	1.920(11)	W(6A)-O(11A)$_{eq.}$	1.890(12)	W(9A)-O(7A)$_{eq.}$	1.868(12)
W(3A)-O(15A)$_{eq.}$	1.922(12)	W(6A)-O(16A)$_{eq.}$	1.888(12)	W(9A)-O(8A)$_{eq.}$	1.941(11)
W(3A)-O(19A)$_{eq.}$	1.884(12)	W(6A)-O(25A)$_{eq.}$	1.969(11)	W(9A)-O(23A)$_{eq.}$	1.900(12)
W(3A)-O(23A)$_{eq.}$	1.942(12)	W(6A)-O(27A)$_{eq.}$	1.887(12)	W(9A)-O(27A)$_{eq.}$	1.902(11)
W(10A)-O(30A)$_{ter.}$	1.731(13)	Cu(1A)-O(24B)$_{ap.}$	2.461(13)	Bi(1A)-(O18A)	2.121(11)
W(10A)-O(31A)$_{ter.}$	1.735(13)	Cu(1A)-O(10A)$_{ap.}$	2.231(12)	Bi(1A)-(O28A)	2.131(11)
W(10A)-O(1A)	2.124(11)	Cu(1A)-O(13A)	1.972(11)	Bi(1A)-O(37A)	2.160(10)
W(10A)-O(20A)	1.998(12)	Cu(1A)-O(4A)	1.942(12)		
W(10A)-O(21A)	2.134(11)	Cu(1A)-O(12A)	1.986(12)		
W(10A)-O(2A)	1.983(12)	Cu(1A)-O(24A).	1.971(11)		

Cu-3b

Bond	d / Å	Bond	d / Å	Bond	d / Å
W(1B)-O(37B)$_{ax.}$	2.181(11)	W(4B)-O(9B)$_{ax.}$	2.241(10)	W(7B)-O(3B)$_{ax.}$	2.249(11)
W(1B)-O(6B)$_{ter.}$	1.719(11)	W(4B)-O(18B)$_{ter.}$	1.745(10)	W(7B)-O(24B)$_{ter.}$	1.730(11)
W(1B)-O(1B)$_{eq.}$	1.826(11)	W(4B)-O(7B)$_{eq.}$	1.894(11)	W(7B)-O(10B)$_{eq.}$	1.948(10)
W(1B)-O(2B)$_{eq.}$	1.787(11)	W(4B)-O(19B)$_{eq.}$	1.955(11)	W(7B)-O(11B)$_{eq.}$	1.994(11)
W(1B)-O(33B)$_{eq.}$	2.000(11)	W(4B)-O(25B)$_{eq.}$	1.897(11)	W(7B)-O(12B)$_{eq.}$	1.966(10)
W(1B)-O(34B)$_{eq.}$	2.106(11)	W(4B)-O(27B)$_{eq.}$	1.903(11)	W(7B)-O(23B)$_{eq.}$	1.800(11)
W(2B)-O(37B)$_{ax.}$	2.283(10)	W(5B)-O(9B)$_{ax.}$	2.225(11)	W(8B)-O(3B)$_{ax.}$	2.258(10)
W(2B)-O(26B)$_{ter.}$	1.703(12)	W(5B)-O(28B)$_{ter.}$	1.738(11)	W(8B)-O(31B)$_{ter.}$	1.719(10)
W(2B)-O(13B)$_{eq.}$	1.948(10)	W(5B)-O(10B)$_{eq.}$	1.900(10)	W(8B)-O(4B)$_{eq.}$	1.918(11)
W(2B)-O(19B)$_{eq.}$	1.877(11)	W(5B)-O(21B)$_{eq.}$	1.804(11)	W(8B)-O(12B)$_{eq.}$	1.932(11)
W(2B)-O(20B)$_{eq.}$	1.960(11)	W(5B)-O(25B)$_{eq.}$	2.003(10)	W(8B)-O(14B)$_{eq.}$	1.926(11)
W(2B)-O(33B)$_{eq.}$	1.878(11)	W(5B)-O(15B)$_{eq.}$	2.003(11)	W(8B)-O(30B)$_{eq.}$	1.942(11)
W(3B)-O(37B)$_{ax.}$	2.316(10)	W(6B)-O(9B)$_{ax.}$	2.267(11)	W(9B)-O(3B)$_{ax.}$	2.233(10)
W(3B)-O(29B)$_{ter.}$	1.735(11)	W(6B)-O(32B)$_{ter.}$	1.736(11)	W(9B)-O(16B)$_{ter.}$	1.717(11)
W(3B)-O(13B)$_{eq.}$	1.922(11)	W(6B)-O(15B)$_{eq.}$	1.908(11)	W(9B)-O(4B)$_{eq.}$	1.975(10)
W(3B)-O(14B)$_{eq.}$	1.884(11)	W(6B)-O(17B)$_{eq.}$	1.934(11)	W(9B)-O(11B)$_{eq.}$	1.922(11)
W(3B)-O(34B)$_{eq.}$	1.838(11)	W(6B)-O(20B)$_{eq.}$	1.867(11)	W(9B)-O(17B)$_{eq.}$	1.897(10)
W(3B)-O(22B)$_{eq.}$	2.028(11)	W(6B)-O(27B)$_{eq.}$	1.954(11)	W(9B)-O(22B)$_{eq.}$	1.841(11)
W(10B)-O(5B)$_{ter.}$	1.715(11)	Cu(1B)-O(17A)$_{ap.}$	2.648(13)	Bi(1B)-O(3B)	2.132(10)
W(10B)-O(8B)$_{ter.}$	1.763(12)	Cu1B)-O(6B)$_{ap.}$	2.202(11)	Bi(1B)-O(9B)	2.144(10)
W(10B)-O(1B)	2.047(11)	Cu(1B)-O(36B)	1.979(12)	Bi(1B)-O(37B)	2.133(11)
W(10B)-O(2B)	2.198(11)	Cu(1B)-O(35B)	2.012(12)		
W(10B)-O(7B)	1.970(11)	Cu(1B)-O(21B)	1.953(11)		
W(10B)-O(30B)	1.962(11)	Cu(1B)-O(23B)	1.937(11)		

Table S6. Bond valence sum (BVS) values for the transition metal centers of **Cu-1**, **Cu-2**, and **Cu-3**.

Cu-1							
Atom	**BVS-Value**	**Atom**	**BVS-Value**	**Atom**	**BVS-Value**	**Atom**	**BVS-Value**
Bi1A	3.2237	W5A	5.8989	Bi1B	3.2093	W5B	6.0019
Cu1A	2.0848	W6A	6.0164	Cu1B	2.0261	W6B	5.9893
W1A	6.0207	W7A	5.9626	W1B	6.0439	W7B	5.9726
W2A	5.9993	W8A	5.9488	W2B	6.0151	W8B	5.9693
W3A	5.9868	W9A	6.0197	W3B	5.9700	W9B	5.9289
W4A	5.9632	W10A	5.9618	W4B	6.0305	W10B	5.9143
Cu-2							
Atom	**BVS-Value**	**Atom**	**BVS-Value**	**Atom**	**BVS-Value**	**Atom**	**BVS-Value**
Bi1A:	3.1824	W5A	6.0483	Bi1B	3.2099	W5B	5.9139
Cu1A:	1.9099	W6A	5.8529	Cu1B	1.9768	W6B	5.9641
W1A	5.9611	W7A	5.8400	W1B	5.9471	W7Bv	5.8783
W2A	6.0447	W8A	5.9944	W2B	6.0712	W8B	5.9760
W3A	6.0040	W9A	6.0923	W3B	5.8620	W9B	5.9739
W4A	6.0379	W10A	5.8905	W4B	5.9172	W10B	5.8848
Cu-3							
Atom	**BVS-Value**	**Atom**	**BVS-Value**	**Atom**	**BVS-Value**	**Atom**	**BVS-Value**
Bi1A	3.1953	W5A	5.9571	Bi1B	3.1872	W5B	5.9215
Cu1A	1.9381	W6A	6.1850	Cu1B	1.9426v	W6B	5.9367
W1A	5.9577	W7A	5.8286	W1B	6.1474v	W7B	5.9117
W2A	5.9520	W8A	5.9810	W2B	6.0669	W8B	5.8887
W3A	5.8540	W9A	6.0381	W3B	5.9293	W9B	6.1306
W4A	5.9347	W10A	5.9226	W4B	5.9761	W10B	6.0228

Table S7. List of selected bond lengths for **Cu-4** (left) and **Cu-5** (right).

Cu-4

Bond	d / Å	Bond	d / Å	Bond	d / Å
W(1)-O(8)$_{ax.}$	2.255(14)	W(4)-O(11)$_{ax.}$	2.233(14)	W(7)-O(13)$_{ax.}$	2.258(15)
W(1)-O(22)$_{ter.}$	1.724(14)	W(4)-O(31)$_{ter.}$	1.729(17)	W(7)-O(29)$_{ter.}$	1.728(16)
W(1)-O(9)$_{eq.}$	1.879(13)	W(4)-O(6)$_{eq.}$	1.853(13)	W(7)-O(10)$_{eq.}$	1.835(13)
W(1)-O(1)$_{eq.}$	1.849(13)	W(4)-O(17)$_{eq.}$	1.989(14)	W(7)-O(12)$_{eq.}$	1.893(15)
W(1)-O(5)$_{eq.}$	1.948(12)	W(4)-O(38)$_{eq.}$	1.993(14)	W(7)-O(18)$_{eq.}$	1.965(12)
W(1)-O(4)$_{eq.}$	1.985(12	W(4)-O(36)$_{eq.}$	1.924(6)	W(7)-O(19)$_{eq.}$	1.985(13)
W(2)-O(11)$_{ax.}$	2.230(13)	W(5)-O(11)$_{ax.}$	2.274(12)	W(8)-O(13)$_{ax.}$	2.278(18)
W(2)-O(21)$_{ter.}$	1.717(13)	W(5)-O(34)$_{ter.}$	1.722(13)	W(8)-O(32)$_{ter.}$	1.73(2)
W(2)-O(2)$_{eq.}$	1.824(12)	W(5)-O(3)$_{eq.}$	1.913(13)	W(8)-O(19)$_{eq.}$	1.900(16)
W(2)-O(3)$_{eq.}$	1.989(12)	W(5)-O(16)$_{eq.}$	1.929(16)	W(8)-O(23)$_{eq.}$	1.907(17)
W(2)-O(17)$_{eq.}$	1.912(16)	W(5)-O(27)$_{eq.}$	1.901(5)	W(9)-O(35)$_{ax.}$	2.243(16)
W(2)-O(9)$_{eq.}$	1.978(15)	W(5)-O(38)$_{eq.}$	1.890(18)	W(9)-O(33)$_{ter.}$	1.694(19)
W(3)-O(8)$_{ax.}$	2.269(17)	W(6)-O(35)$_{ax.}$	2.257(13)	W(9)-O(14)$_{eq.}$	1.842(13)
W(3)-O(26)$_{ter.}$	1.693(18)	W(6)-O(30)$_{ter.}$	1.727(14)	W(9)-O(15)$_{eq.}$	1.910(6)
W(3)-O(16)$_{eq.}$	1.915(15)	W(6)-O(7)$_{eq.}$	1.827(12)	W(9)-O(24)$_{eq.}$	1.981(14)
W(3)-O(4)$_{eq.}$	1.930(14)	W(6)-O(12)$_{eq.}$	1.954(16)	W(9)-O(25)$_{eq.}$	1.946(15)
Cu(1)-O(39)	2.22(3)	W(6)-O(28)$_{eq.}$	1.960(14)	Cu(1)-Cu(2)	4.8831(42)
Cu(1)-O(14)	1.932(14)	W(6)-O(25)$_{eq.}$	1.965(18)	Cu(2)-Cu(2)	4.8333(27)
Cu(1)-O(6)	1.936(13)	Bi(1)-O(11)	2.111(12)		
Cu(2)-O(40)	2.170(15)	Bi(1)-O(8)	2.092(19)		
Cu(2)-O(1)	1.930(13)	Bi(2)-O(13)	2.82(2)		
Cu(2)-O(2)	1.952(14)	Bi(2)-O(35)	2.099(13)		
Cu(2)-O(10)	1.928(13)				

Cu-5

Bond	d / Å	Bond	d / Å	Bond	d / Å
W(1)-O(4)$_{ax.}$	2.259(8)	W(2)-O(3)$_{ax.}$	2.260(8)	W(3)-O(3)$_{ax.}$	2.227(9)
W(1)-O(10)$_{ter.}$	1.730(10)	W(2)-O(13)$_{ter.}$	1.726(10)	W(3)-O(15)$_{ter.}$	1.728(10)
W(1)-O(16)$_{eq.}$	1.824(9)	W(2)-O(2)$_{eq.}$	1.845(10)	W(3)-O(12)$_{eq.}$	1.955(10)
W(1)-O(19)$_{eq.}$	1.966(7)	W(2)-O(14)$_{eq.}$	1.918(4)	W(3)-O(5)$_{eq.}$	1.932(9)
W(1)-O(7)$_{eq.}$	2.005(9)	W(2)-O(12)$_{eq.}$	1.966(11)	W(3)-O(1)$_{eq.}$	2.013(9)
W(1)-O(5)$_{eq.}$	1.912(9)	W(2)-O(9)$_{eq.}$	1.974(10)	W(3)-O(6)$_{eq.}$	1.828(9)
W(4)-O(3)$_{ax.}$	2.269(9)	W(5)-O(4)$_{ax.}$	2.296(13)	Cu(1)-O(8)$_{ap.}$	2.234(14)
W(4)-O(17)$_{ter.}$	1.727(10)	W(5)-O(8)$_{ter.}$	1.720(13)	Cu(1)-O(6)$_{eq.}$	1.951(10)
W(4)-O(9)$_{eq.}$	1.944(10)	W(5)-O(7)$_{eq.}$	1.889(9)	Cu(1)-O(16)$_{eq.}$	1.959(10)
W(4)-O(1)$_{eq.}$	1.904(10)	W(5)-O(11)$_{eq.}$	1.911(9)	Cu(1)-Cu(4)	2.76(2)
W(4)-O(18)$_{eq.}$	1.908(3)	Bi(1)-O(3)	2.114(8)	Cu(1)-Cu(3)	2.871(12)
W(4)-O(11)$_{eq.}$	1.917(9)	Bi(1)-O(4)	2.080(12)	Cu(4)-O(16)$_{eq.}$	2.058(11)
Cu(2)-O(2)$_{eq.}$	1.935(10)	Cu(3)-O(2)$_{eq.}$	1.970(14)	Cu(4)-Cu(1)	2.76(2)
Cu(2)-Cl	2.557(13)	Cu(3)-O(6)	2.121(14)		
		Cu(2)-Cu(3)	2.755(13)		

Table S8. BVS values for **Cu-4** and **Cu-5**.

Cu-4

Atom	BVS-Value	Atom	BVS-Value	Atom	BVS-Value
Bi1	3.3133	W3	6.0345	W9	6.0987
Bi2	3.3683	W4	5.7934	W10	5.9270
Cu1	2.0968	W5	6.0465		
Cu2	2.1038	W6	5.8981		
W1	6.0325	W7	5.9672		
W2	5.9913	W8	6.0710		

Cu-5

Atom	BVS-Value	Atom	BVS-Value
Bi1	3.2899	W4	5.9701
Cu1	2.0147	W5	6.1400
Cu2	2.1030		
W1	5.9084		
W2	5.9256		
W3	5.8974		

Table S9. List of selected bond lengths (left) and BVS values (right) for **Cu-6**.

Cu-6							Cu-6					
Bond	**d / Å**	**Bond**	**d / Å**	**Bond**	**d / Å**		**Atom**	**BVS-Value**	**Atom**	**BVS-Value**	**Atom**	**BVS-Value**
W(1)-O(15)$_{ax.}$	2.238(4)	W(4)-O(13)$_{ter.}$	1.723(5)	Cu(1)-O(12)	2.4727(0)		Bi1A	3.2237	W5A	5.8989	Bi1B	3.2093
W(1)-O(10)$_{ter.}$	1.736(5)	W(4)-O(9)$_{ter.}$	1.777(4)	Cu(1)-O(9)	1.907(5)		Cu1A	2.0848	W6A	6.0164	Cu1B	2.0261
W(1)-O(3)$_{eq.}$	1.878(4)	W(4)-O(3)	2.329(4)	Cu(1)-OW$_1$	1.962(5)		W1A	6.0207	W7A	5.9626	W1B	6.0439
W(1)-O(4)$_{eq.}$	1.959(4)	W(4)-O(2)	2.078(4)				W2A	5.9993	W8A	5.9488	W2B	6.0151
W(1)-O(6)$_{eq.}$	2.105(4)	W(4)-O(7)	1.948(4)				W3A	5.9868	W9A	6.0197	W3B	5.9700
W(1)-O(8)$_{eq.}$	1.789(4)	W(4)-O(9)	1.777(4)				W4A	5.9632	W10A	5.9618	W4B	6.0305
W(2)-O(15)$_{ax.}$	2.264(4)	W(5)-O(21)$_{ter.}$	1.747(4)				W5B	6.0019				
W(2)-O(20)$_{ter}$	1.717(4)	W(5)-O(11)$_{ter.}$	1.745(5)				W6B	5.9893				
W(2)-O(2)$_{eq.}$	1.830(4)	W(5)-O(5)	2.213(4)				W7B	5.9726				
W(2)-O(5)$_{eq.}$	1.898(4)	W(5)-O(8)	2.198(4)				W8B	5.9693				
W(2)-O(4)$_{eq.}$	1.933(4)	W(5)-O(16)	1.959(4)				W9B	5.9289				
W(2)-O(17)$_{eq.}$	2.043(4)	W(5)-O(18)	1.887(4)				W10B	5.9143				
W(3)-O(15)$_{ax.}$	2.243(4)	W(6)-O(12)$_{ter.}$	1.749(4)									
W(3)-O(19)$_{ter.}$	1.716(4)	W(6)-O(14)$_{ter.}$	1.747(4)									
W(3)-O(1)$_{eq.}$	1.949(4)	W(6)-O(7)	1.891(5)									
W(3)-O(6)$_{eq.}$	1.877(5)	W(6)-O(3)	2.236(4)									
W(3)-O(17)$_{eq.}$	1.875(4)	W(6)-O(16)	1.912(4)									
W(3)-O(18)$_{eq.}$	1.967(4)	W(6)-O(5)	2.265(4)									

3 POMs based on a {B-*β*-$BiW_{10}O_{37}$} subunit

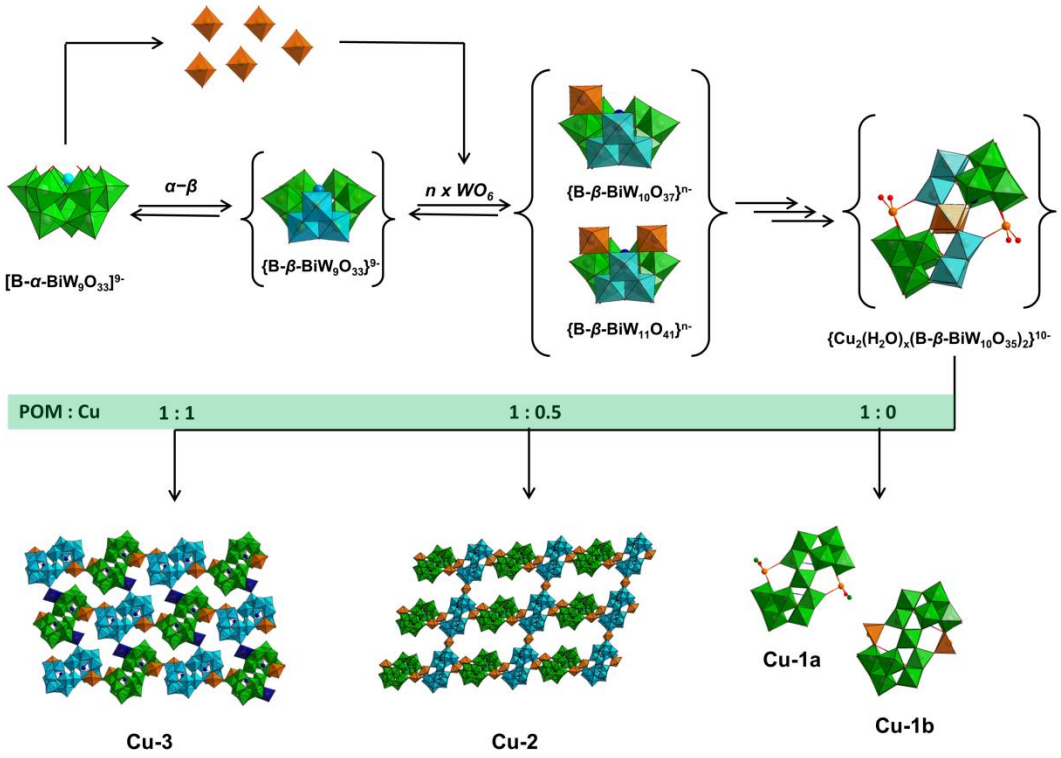

Figure S1. Schematic formation of Cu substituted Krebs-type POMs.

In all of the Krebs-type structures **Cu-1**, **Cu-2**, and **Cu-3**, the first coordination sphere of the Bi heteroatom is located in a pyramidal coordination environment with Bi–O bond lengths in the range between 2.117(8) Å and 2.160(10) Å and angles between (84.2-88.7°) for the the Bi–O_{ax} bonds. The same labeling scheme was used for tungsten atoms in the structures **Cu-1** – **Cu-3**. The tungsten atoms W(1)-W(9) represent the hypothetical {$BiW_{10}O_{37}$} unit where they are in a distorted octahedral coordination environment with W–O bond lengths between 1.695(13) Å and 1.765(13) Å (terminal oxygen atoms), between 1.783(10) Å and 2.198(11) Å (equatorial O atoms), and between 1.735(10) Å and 2.337(8) Å for the axial oxygen atoms. The tungsten atom W(10) as a part of the transition metal core, displays a slightly different coordination environment with W–O bonds ranging from 1.715(11) Å to 2.198(11) Å. Intermetallic W···W distances are in the range of 3.2425(1) Å to 3.5010(1) Å between edge sharing WO_6 octahedra and between 3.6368(1) Å and 3.7137(1) Å for corner sharing WO_6 octahedra. The W···W

distance to the ligand bridging WO_6 octahedron of W(10) is slightly longer (3.5479(1) Å – 3.9417(1) Å). The oxidation state of the metal cations of the polyanion was checked by BVS analysis,[23] and an oxidation state of +II for Cu, +VI for W and +III for Bi was confirmed (Table S3-Table S5 and Table S6).

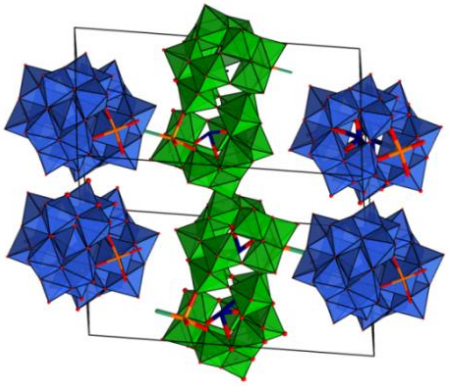

Figure S2. Arrangement of the polyanions **Cu-1a** (green) and **Cu-1b** (blue) in the unit cell; crystal water molecules and counter-cations have been omitted for clarity.

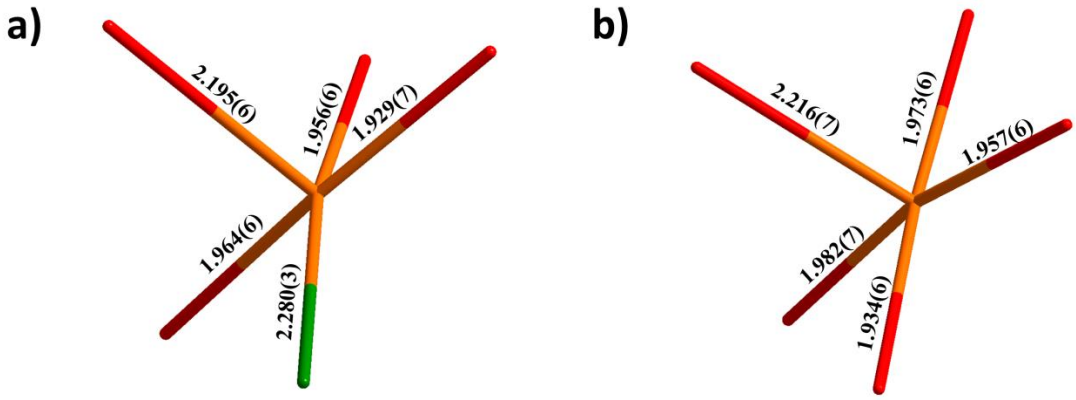

Figure S3. Coordination geometry of Cu(II) cations in the transition metal belt of **Cu-1a** (a) and **Cu-1b** (b).

The Cu center of **Cu-1b** is found in an almost square pyramidal coordination environment. It is coordinated by two water ligands with Cu–O bond lengths of 1.982(7) Å and 1.973(6) Å as well as by two oxygen atoms of the [B-β-BiW_9O_{33}]$^{9-}$ subunit with slightly shorter Cu–O bond lengths

(1.957(6) Å and 1.934(6) Å). A fifth oxygen atom is located in the apical position with a Cu–O bond length of 2.216(7) Å. In the coordination sphere of **Cu-1a**, one of the crystal water molecules is substituted by a chloride ligand which leads to a distortion of the square pyramidal coordination geometry. The Cl^- ion is found at a distance of 2.280(3) Å from the Cu (II) center, coplanar with the coordinating water ligand (1.964(6) Å) and the two terminal oxygen atoms of the {B-β-BiW_9O_{33}} subunit at 1.956(6) Å and 1.929(7) Å, respectively. The apical position of the distorted pyramid is occupied by another oxygen atom of the subunit at 2.195(6) Å (Figure S3). The presence of the Cl^- ligand leads to slightly shorter Cu–O bonds. A total of 11 Na^+ counter-cations and 83 crystal water molecules have been refined between the two isolated polyanions **Cu-1a** and **Cu-2b** which are not connected by additional Cu(II) cations. Each Na^+ site was found to be fully occupied.

The two POM monomers in the 1D-chains of **Cu-2** and **Cu-3** are bridged via the Cu(II) ion of the transition metal belt to a terminal oxygen atom of the adjacent monomer (Figure 2). The two CuO_6 octahedra of the monomers are shown in orange. The resulting 1D-chains are connected into a 2D layer by additional chain-bridging Cu(II) cations (orange octahedra). Figure 2 provides an overview of the connectivity in the layers of **Cu-2** and **Cu-3**.

The bridging Cu atom in **Cu-2** is located on the $\bar{1}$ symmetry site, and its octahedral coordination environment contains four crystal water molecules in the equatorial plane with an average Cu–O bond length of 1.966 Å. The axial positions of the CuO_6 octahedron are occupied by the terminal oxygen atoms of the tungsten atom at a distance of 2.3294(1) Å. Bridging in **Cu-3** occurs via 2 Cu atoms and through terminal oxygen atoms of different tungsten centers of the repeating unit compared to the arrangement in **Cu-2**, thus resulting in a different 2D network from **Cu-2**. The Cu···Cu distances between the copper atoms of the polyanions **Cu-1**, **Cu-2**, and **Cu-3** are generally in the same range between 10.0269(1) Å and 10.276(3) Å.

4 POMs based on the [B-α-BiW_9O_{33}]$^{9-}$ building block

4.1 Detailed structural analysis of Cu-4 and Cu-5

Cu-4 and **Cu-5** crystallize in the monoclinic space group $P2_1/m$ and in the tetragonal space group $P\bar{4}2_1m$, respectively. Crystal structure refinement reveals the presence of a tungstobismuthate of the type $[Cu_3(H_2O)M(Q)_3(B\text{-}\alpha\text{-}BiW_9O_{33})_2]^{n-}$ (M = Rb, K or Cu; Q = H_2O or Cl; n = 12). While M and Q can be defined clearly in **Cu-4**, disorder in the transition metal belt of **Cu-5** indicates that it is composed of polyanions with different belt compositions (§4.2). **Cu-5** consists of single polyanions linked into a 3D-network, while the polyanions in **Cu-4** crystallize without Cu–O–W bridging.

The polyanions constituting **Cu-4** and **Cu-5** are isostructural. The Bi heteroatom coordinates to 3 oxygen atoms with Bi–O bond lengths between 2.080(12) Å and 2.114(8) Å and Bi–O bond angles between 86.1(3) and 88.3(7)°. All tungsten atoms exhibit distorted octahedral coordinations with bond lengths between 1.693(18) Å and 1.730(10) Å for the terminal oxygen atoms, 1.824(9) Å and 2.013(9) Å for equatorial O atoms, and between 2.227(9) Å and 2.296(13) Å for the axial oxygen atoms. Intermetallic W···W distances between edge sharing WO_6 octahedra are in the range of 3.3163(8) Å to 3.3431(7) Å and range from 3.6910(8) Å to 3.7153(11) Å for corner sharing WO_6 octahedra.

The fully occupied Cu(II) positions Cu(1) and Cu(2) in **Cu-4** and **Cu-5** form a triangle with Cu–Cu–Cu angles between 59.326(43)° and 60.337(38)° and interatomic Cu···Cu distances between 4.8831(42) Å and 4.935(24) Å. Interatomic distances in **Cu-5** between the fully occupied Cu(II) positions and the disordered Cu(II) sites Cu(3) and Cu(4) are between 2.755(13) Å and 2.871(12) Å.

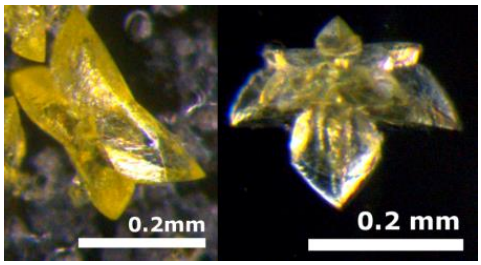

Figure S4. Representative image of **Cu-5** crystals recorded on a stereomicroscope.

4.2 Detailed description of the Cu/K disorder in Cu-5

While **Cu-4** does not display disorder, the transition metal belt of 3D-$K_{6.56}Cu_{0.43}H_{2.20}[(Cu_3Cl)(K_{2.62}Cu_{0.38}(H_2O)_3(B\text{-}\alpha\text{-}BiW_9O_{33})_2]\cdot 13H_2O$ (**Cu-5**) shows a high degree of disorder. This renders the unambiguous assignment of counter-cations difficult.

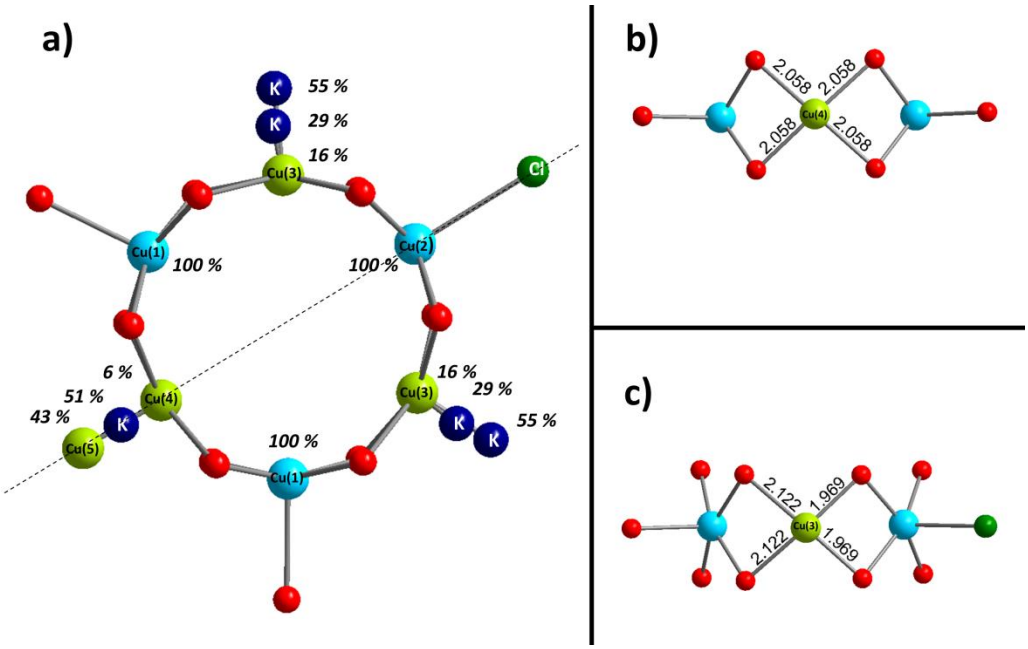

Figure S5. (a) Ball and stick representation of the transition metal core of **Cu-5**. **(b)** Coordination environment of Cu(4). **(c)** Coordination environment of Cu(5). Color code: O = red = O, Cl = dark green, K = dark blue, Cu (disordered) = green, Cu (100 %) = blue.

Compared to **Cu-4** where cavities between Cu atoms are fully occupied by Rb^+ cations, the cavities in **Cu-5** are occupied with K^+, Cu(II) cations and coordinating water ligands which are found on disordered positions. The water ligands of the disordered Cu(II) cations have not been included in the model. This disorder is indicated by residual electron density maxima in the cavities between Cu(1) and Cu(2) and between Cu(1) and Cu(1), respectively,which are less than 1.0 Å apart. Given the position of the electron density maxima in the cavities between Cu(1) and Cu(1') with distances to O atoms between 1.970(14) and 2.121(14) Å and the square planar coordination geometry, the peak was refined as Cu atom Cu(3). The electron density maximum between Cu(2) and Cu(1) was found in a similar coordination environment with Q–O bond lengths of 2.058(11) Å and it was therefore refined as Cu(4). The occupancies of the only

partially occupied Cu(3) and Cu(4) sites were refined to 0.160(04) for Cu(3) and 0.065(04) for Cu(4) which indeed is very small. In the cavity where Cu(4) is located, another electron density maximum without a specific coordination environment or characteristic bond distances was found. In line with the overall Cu content determined by elemental analysis this electron density was refined as Cu(5) with occupancy 0.425(04) This assignment is supported by the atomic displacement parameters which are in agreement with this atom type.

The cavities between Cu(2)/Cu(1) and Cu(1)/Cu(1) are alternatively filled with K^+ and Cu(II) cations. They were summed up to 1 using the linear restraints (SUMP instruction).

4.3 Analytical characterization of Cu-5

4.3.1 Magnetic susceptibility of Cu-5

Fitting the data using the Curie-Weiss law (1) did not lead to satisfactory results at low temperature. Using a model which was previously reported and used to fit the data for the 3D network structure $Na_9[Cu_3Na_3(H_2O)_9(B\text{-}\alpha\text{-}AsW_9O_{33})_2]$ provided better results (2).[24,25]

$$\chi_m = \frac{C}{T-\Theta} \qquad (1)$$

χ_m = molar magnetic susceptibility, C = Curie constant, T = Temperature, Θ = Curie temperature

$$\chi_m = \frac{Ng^2\beta^2}{4k(T-\Theta)}\left(\frac{1+5\exp\left(\frac{3J}{kT}\right)}{1+\exp\left(\frac{3J}{kT}\right)}\right) \qquad (2)$$

The best least squares fit is achieved with the spin-exchange factor J = -7500 cm^{-1}, a Curie temperature θ = -1.58 K and a Landé g tensor g = 4.65, (β = Bohr magneton).

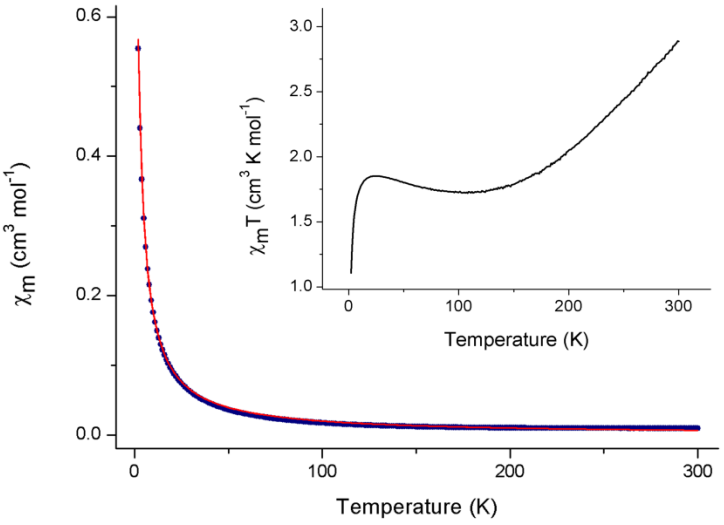

Figure S6. Temperature dependence χ_m vs. T of **Cu-5** between 2 and 200 K at 500 Oe (**inset:** χ_m x T vs. T).

4.3.2 Powder X-ray diffractogram of Cu-5

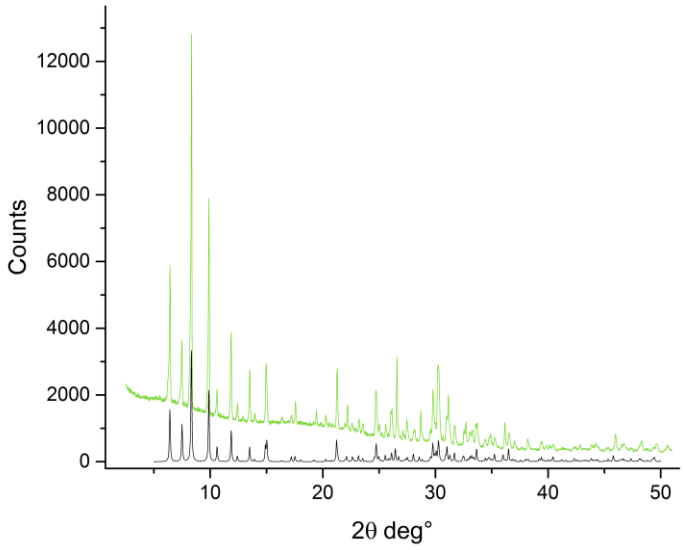

Figure S7. PXRD pattern of **Cu-5** (Cu $K_{\alpha 1}$): calculated (black), measured (green).

4.3.3 High resolution mass spectrometry of Cu-5

The average structural information obtained from single crystal X-ray structure determination leaves the question open as to whether the polyanions $\{Cu_5(H_2O)_4Cl(BiW_9O_{33})_2\}$ and $\{Cu_6(H_2O)_5Cl(BiW_9O_{33})_2\}$ truly exist. The distinction between polyanions with different cores should in principle be possible by high resolution mass spectrometry through their specific masses giving rise to distinct signals. The distribution of the different polyanion species was estimated from the refined site occupancies in the transition metal belt. However, it is only possible to give a maximum percentage of $[Cu_3(H_2O)_2Cl(BiW_9O_{33})_2]^{12-}$ (62%) if the remaining polyanions have a $[Cu_4(H_2O)_3Cl(BiW_9O_{33})_2]^{10-}$ structure (38%). Polyanions with a Cu5 or Cu6 core are not considered in this limiting case. A determination of the actual distribution requires follow-up studies. The occurrence of polyanions with a Cu5 or Cu6 core cannot be calculated from the refined occupancies (Table S10). The HR-ESI-MS peak with z = 5- was analyzed in detail. The polyanion $[Cu_3(H_2O)_3(BiW_9O_{33})_2]^{12-}$ contains cavities which are filled alternately with K^+ or Cu^{2+} cations. Whether these cations should be considered as part of the structure is unresolved from structural data, but important for the assignment of specific peaks to polyanion structures. A large number of different $[Cu_3(H_2O)_xCl_{3-x}Cu_yK_{3-y}(BiW_9O_{33})_2]$ - $a{\cdot}K$ $b{\cdot}H\}^{5-}$ (x = 0-3, y = 0-3) polyanions may be detected and potassium adducts may form with the polyanions, i.e.

the values of *a* and *b* need to be adjusted to an overall polyanion charge of 5-. Due to the formation of K^+ adducts and an unknown number of water ligands or Cl^- coordinating to the transition metal core, a variety of species may be detected. This leads to an overlap of the signals from the different species and does not allow the unambiguous identification of a specific polyanion.

Table S10. List of possible species to be observed in the HR-ESI MS of **Cu-5.**

Fragment	**Mass**	**Occurrence[a]**
$\{Cu_3(H_2O)_2Cl(BiW_9O_{33})_2\}^{12-}$	5044.52	max. 62%
$\{Cu_4(H_2O)_3Cl(BiW_9O_{33})_2\}^{10-}$	5126.46	max. 38%
$\{Cu_5(H_2O)_4Cl(BiW_9O_{33})_2\}^{8-}$	5208.40	---
$\{Cu_6(H_2O)_5Cl(BiW_9O_{33})_2\}^{7-}$	5272.44	---

[a] Assuming the scenario of only polyanions with Cu3 and Cu4 cores being present.

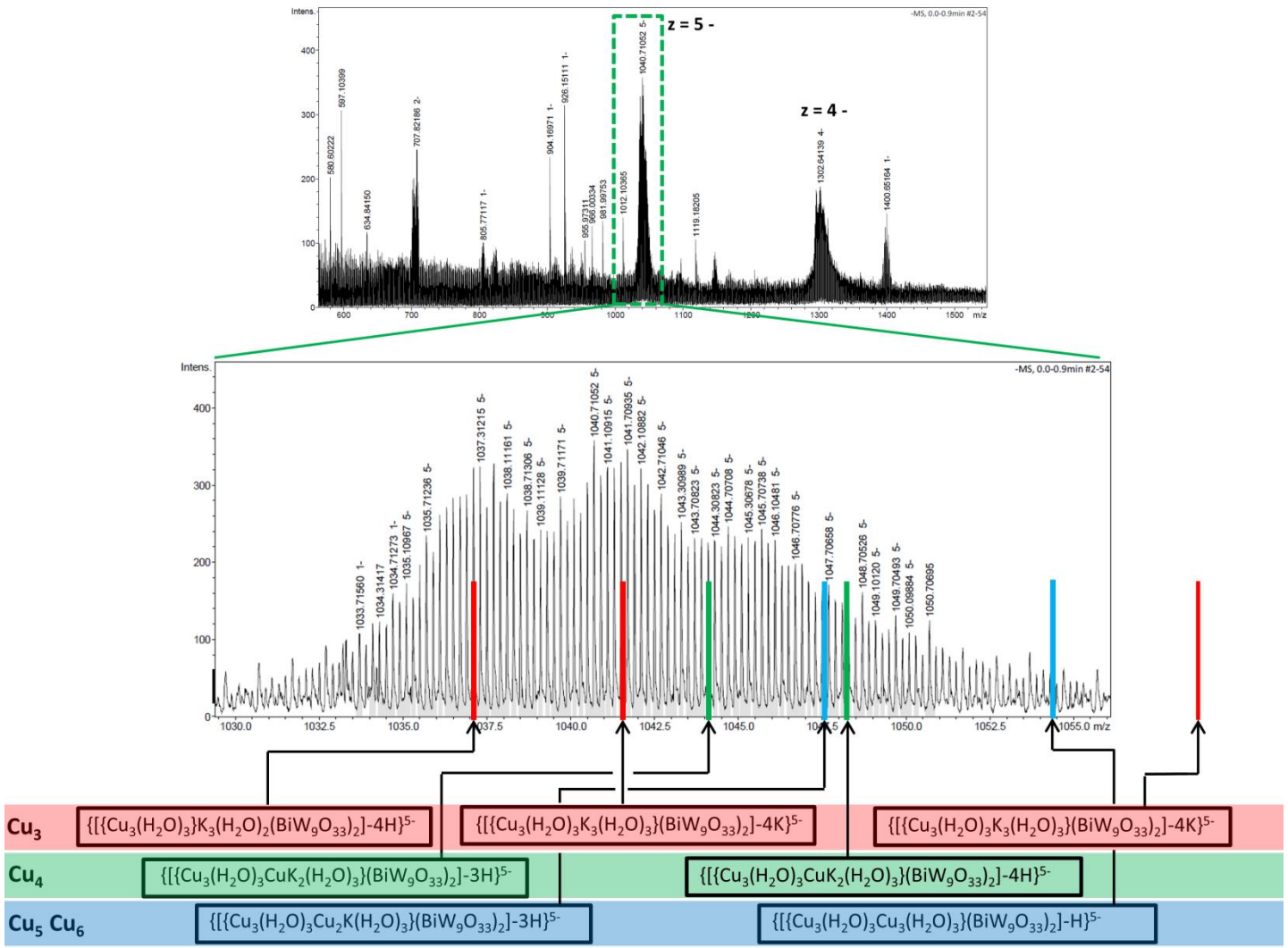

Figure S8. HR-ESI-MS of **Cu-5** with positions of different possible heteropolyanions with their possible K/H adducts; blue = Cu_5, Cu_6 cores, green = Cu_4 cores, red = Cu_3 cores.

5 Photocatalytic properties of Cu-5

All catalytic tests were performed in 10 mL headspace vials, sealed with a natural rubber septum (VWR) and a crimp cap (Supelco). Catalytic test solutions were irradiated under stirring with a blue LED (460 nm 4650 Lux). O_2 evolution was monitored with a Clark sensor (OX-N) from Unisense and quantified by GC (Agilent Technologies 7820A gas chromatograph, with helium 6.0 purity). H_2 evolution was monitored with a Clark-type H_2 sensitive sensor (H2-NP) from Unisense and quantified by GC (Varian CP 3800 Gas Chromatograph). The sensors were calibrated prior to each experiment with a two point calibration using a sample with known concentrations of O_2/H_2. In order to quantify the amount of hydrogen produced during catalysis, gas samples from the headspace were analyzed by gas chromatography.

5.1 Photocatalytic O_2 evolution

$[Ru(bpy)_3]Cl_2$ was used as photosensitizer (PS) and $Na_2S_2O_8$ as sacrificial electron acceptor. The catalytic activity was tested in three different buffer solutions (acetate pH = 4.75; NaPi pH = 7.0; borate pH = 8.0 at 100 µM buffer concentration). This covers a pH range in which O_2 evolution has been reported previously for similar polyoxometalate-based water oxidation catalysts. The formation of a solid precipitate (POM-PS complex) was observed in all photocatalytic tests. Previous studies have investigated such POM-PS complex formation through electrostatic interactions of the negatively charged polyanion and the positively charged photosensitizer cation $[Ru(bpy)_3]^{2+}$ in more detail.[26–32] The observed characteristic FT-IR bands of the POM-PS complex can be assigned to the polyanion and to the ruthenium sensitizer, respectively. The elemental composition was analyzed by an EDX mapping which indicates the presence of larger tungsten containing domains, probably due to residual undissolved **Cu-5** (Figure S9).

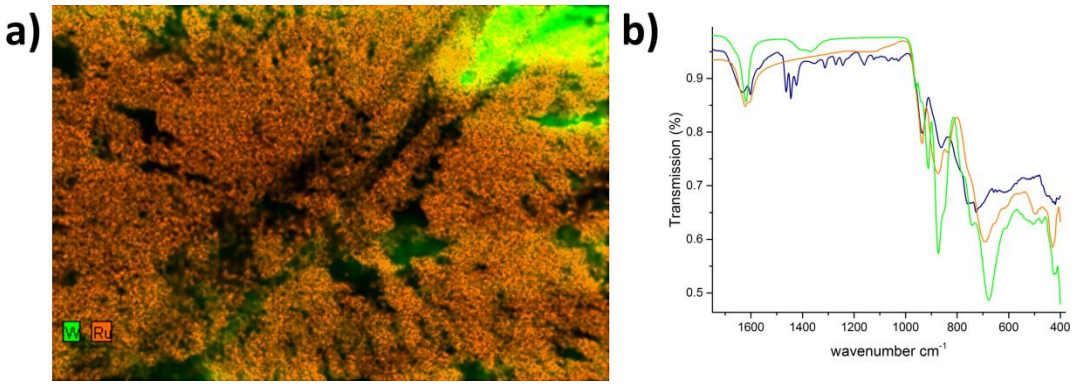

Figure S9. (**a**) EDX mapping of the PS-complex (magnification 230x) showing the distribution of W and Ru. (**b**) FT-IR spectrum of the PS complex of **Cu-5** (blue) vs. pristine **Cu-5** (orange) and $Na_9[BiW_9O_{33}]\cdot 19.5\ H_2O$ (green).

5.2 Photocatalytic H_2 evolution

An ascorbate buffer system at pH 4 was prepared in demineralized water (8.0 mL), and ascorbic acid (88.0 mg, 0.499 mmol) and sodium ascorbate (98.0 mg, 0.494 mmol) were added for a total buffer concentration of 0.12 M. $[Ru(bpy)_3]Cl_2\cdot 6H_2O$ (1 mM) was used as photosensitizer according to previous standard protocols.[32,33] The catalyst was dissolved in 1.0 mL of the prepared buffer solution and added dropwise, affording turbid solutions in the presence of the photosensitizer due to POM-PS complex formation (see Figure S1). This phenomenon was observed in catalytic tests with **Cu-5** as well as in catalytic tests with $[BiW_9O_{33}]^{9-}$. All catalytic tests were prepared under exclusion of light and purged with Ar gas for 15 min prior to irradiation with a blue LED (λ = 470 nm, 4650 LUX).

Table S11. Results of photocatalytic tests with **Cu-5**, **BiW_9**, and blank measurements.

Compound	Concentration (µM)	H_2 (µL)	TON[a]
Cu-5	10.7	65.2	16.4
Cu-5	23.0	55.9	1.6
Cu-5	48.6	46.4	5.5
Cu-5	104.0	40.1	0.5
$Blank_{(max)}$	---	39.1	---
$Blank_{(min)}$	---	29.9	---
BiW_9	12.3	114.1	34.4
BiW_9	23.8	41.0	8.8
BiW_9	25.8	41.1	8.1
BiW_9	55.1	152.8	11.3
BiW_9	73.3	131.7	7.0
BiW_9	108.9	128.6	4.6
BiW_9	122.8	112.1	3.4
BiW_9	148.7	99.5	2.4
$CuSO_4$	25.0	21.9	0
$CuSO_4$	100.0	7.03	0
$CuSO_4$	150.0	12.2	0

[a] TONs were calculated after subtraction of the background contribution to the total amount of H_2.

For **Cu-5** concentrations in the range of 12.5 – 100 µM, formation of 41 to 65 µL H_2 was observed, i.e. values slightly above the background in the absence of catalyst (Table S11). The highest TON was obtained for 10.7 µM **Cu-5** (TON = 31.2). Reference experiments with the lacunary precursor $[B\text{-}\alpha\text{-}BiW_9O_{33}]^{9-}$ afforded an approximately three-fold higher catalytic activity at a catalyst concentration of 50.0 µM with respect to molar H_2 formation and an approx. double TON compared to **Cu-5**. Catalytic tests with lower **BiW_9** concentrations (≤ 50 µM) show a high variance due to difficulties in sample preparation for the particularly low amounts of catalyst (approximately 0.2-0.5 mg). The lower evolved H_2 quantities and TONs for **Cu-5** compared to **BiW_9** shows that Cu-functionalization is not a straightforward strategy to improve tungstobismuthate based H_2 evolution catalysts. The POM-PS complex (cf. above) of **Cu-5** and $[Ru(bpy)_3]^{2+}$ photosensitizer can be considered as potential active species according to previous studies.[28,30,31] Therefore, it was collected by centrifugation, air dried and characterized by FT-IR spectroscopy and EDX analysis (Figure S9). Catalyst recycling experiments were then performed in a fresh solution of ascorbate buffer with $[Ru(bpy)_3]Cl_2$, where the POM-PS complex (497 µg) was added instead of the pristine catalyst and dispersed by sonication for 30 min. Subtraction of

the background H_2 formation by $[Ru(bpy)_3]^{2+}$ demonstrated that no additional H_2 amounts are formed in the presence of the recycled catalyst.

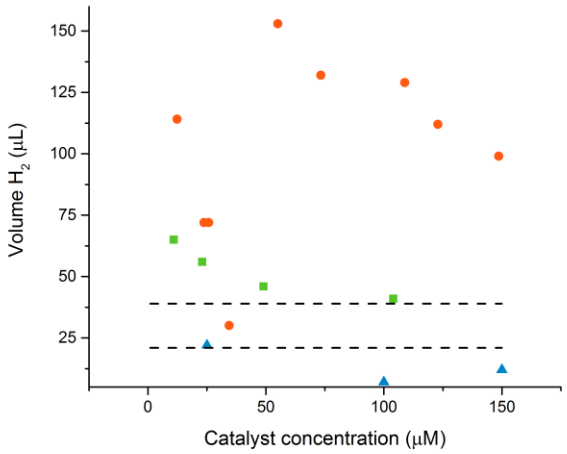

Figure S10. H_2 yields quantified by GC analysis of **Cu-5** (green), $CuSO_4 \cdot 5H_2O$ (blue), and **BiW_9** (red); the dotted line shows the maximal/minimal amount of H_2 formed in absence of catalyst. Conditions: ascorbate buffer (1.2 M, pH = 4.0), $[Ru(bpy)_3]Cl_2$ (1 mM), irradiation by LED (460 nm 4650 LUX).

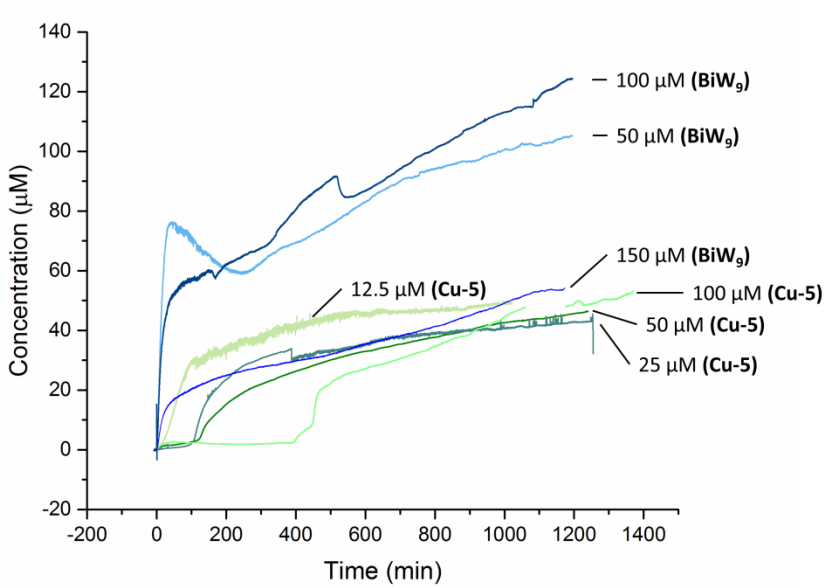

Figure S11. Time dependent H_2 evolution measured with a H_2 sensitive Clark-type sensor: 50-150 µM $[BiW_9O_{33}]^{9-}$ (blue), 12.5-100 µM **Cu-5** (green).

6 The structure of Cu(II) bridged paratungstate B (Cu-6)

The paratungstate B structure is composed of two different subunit types, namely the cap-type $\{HW_3O_{13}\}$ in which three WO_6 octahedra share a common O atom (W–O bond lengths, terminal: 1.716(4)-1.736(5) Å; axial 2.238(4)-2.264(4) Å; equatorial: 1.789(4)-2.105(4) Å) and a $\{W_3O_{14}\}$ unit of three edge sharing WO_6 octahedron without any shared oxygen atom (Figure S12; W–O bond lengths, terminal: 1.723(5)-1.777(4) Å; equatorial: 1.777(4)-2.329(4) Å). Bridging of monomeric $[H_2W_{12}O_{40}]^{10-}$ units occurs via coordination to a Cu(II) ion with Jahn-Teller distorted octahedral coordination geometry.

A total of 4 sodium and 4 potassium counter-cations were refined according to their coordination geometry. Charge balance is achieved by taking into account two hydrogen atoms coordinating to the oxygen atoms O(15) inside of the polyanion. The presence of hydrogen atoms was established earlier by neutron diffraction studies.[34]

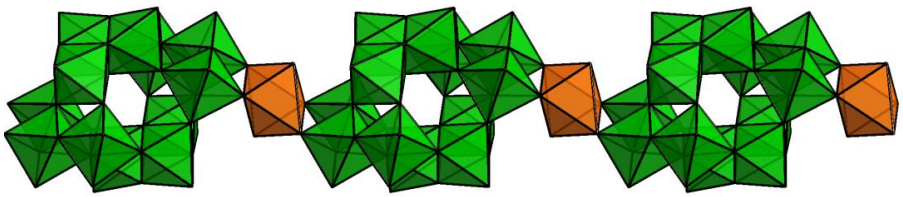

Figure S12. Polyhedral ball-and stick representation of **Cu-6.**

7 Experimental

7.1 Preparation of single crystals

All chemicals were obtained commercially and used without further purification. The lacunary precursor $Na_9[BiW_9O_{33}]\cdot 19.5H_2O$ was prepared according to published procedures and characterized by FT-IR spectroscopy.[35] Repeated syntheses of this precursor showed that these commonly used protocols may also result in the formation of $[W_{12}O_{42}]^{12-}$ or $[Bi_2W_{22}O_{76}]^{12-}$. Furthermore this precursor may contain a small amount of an insoluble impurity which cannot be detected by IR or PXRD. It can be removed from the reaction mixture prior to the addition of the counter cation by filtration over celite. The repeated synthesis of this precursor has shown that it is difficult to isolate it phase pure. Polyanions which have been isolated instead, indicate that α-β isomerization or decomposition of the desired $Na_9[BiW_9O_{33}]\cdot 19.5H_2O$ precursor frequently occurs. Recrystallization for purification may therefore not be possible.

All reported procedures in the following resulted in the formation of at least one high quality single crystal for structure analysis. Formation of phase pure bulk material could **only** be confirmed for **Cu-5** by PXRD analysis.

7.2 Source of $Na_{12}[Cu_2(H_2O)_4Cl_2(B\text{-}\beta\text{-}BiW_{10}O_{35})_2]\cdot 36.5\ H_2O$ / $Na_{10}[Cu_2(H_2O)_6(B\text{-}\beta\text{-}BiW_{10}O_{35})_2]\ 36.5\ H_2O$ (Cu-1)

A solution of $Na_9[BiW_9O_{33}]\cdot 19.5\ H_2O$ (4.00 g, 1.65 mmol) was prepared in demineralized H_2O (40 mL). The starting material $Na_9[BiW_9O_{33}]\cdot 19.5\ H_2O$ may contain minor amounts of an insoluble impurity which was removed by filtration over celite. A solution of $CuSO_4\cdot 5H_2O$ (20 mL, 2.4 mM) was added dropwise under vigorous stirring at room temperature, the colorless solution thereby becomes green. During the addition of the copper sulfate solution, a solid precipitated which was removed by centrifugation. A solution of saturated KCl was added dropwise to the stirred reaction mixture until a solid precipitated which re-dissolved after a few seconds. The green solution was left for crystallization, which led to the formation of crystals of **Cu-1**.

7.3 Source of 2D-$Na_7K_3Cu_{0.5}Cl[Cu_2(H_2O)_4(B\text{-}\beta\text{-}BiW_{10}O_{35})_2]\cdot 29.5H_2O$ (Cu-2), 2D-$Na_{5.5}K_{2.5}Cu[Cu_2(H_2O)_4(B\text{-}\beta\text{-}BiW_{10}O_{35})_2]\cdot 17.5H_2O$ (Cu-3), and $Na_6Rb_6[Cu_3(H_2O)_3(B\text{-}\beta\text{-}BiW_9O_{33})_2]\cdot 21H_2O$ (Cu-4) crystals

Crystals of **Cu-2**, **Cu-3** and **Cu-4** were obtained from the same reaction mixture by adding different counter-cations.

A solution of of $Na_9[BiW_9O_{33}]\cdot 19.5\ H_2O$ (1.00 g, 0.41 mmol) was prepared in demineralized H_2O (10 mL). The starting material $Na_9[BiW_9O_{33}]\cdot 19.5\ H_2O$ may contain a small amount of an insoluble impurity which was removed by filtration over celite. A solution of $CuSO_4\cdot 5H_2O$ (10 mL, 1.2 mM) was added dropwise to the stirred reaction mixture at room temperature. During the addition, the color changed to green. The pH after the addition was 5.3. The reaction mixture was divided into 2 parts of 10 mL.

Cu-2 and **Cu-3:** A saturated solution of KCl was added to the stirred reaction mixture until a solid precipitated which was removed by filtration over celite. The reaction mixture was left for crystallization. Crystals of **Cu-2** and **Cu-3** form simultaneously with an unidentified green slurry. The crystals were removed carefully from this slurry and stored in a saturated solution of KCl.

Cu-4: A solution of RbCl (1.0 M) was added dropwise to the stirred reaction mixture until a solid formed which was removed by filtration. The green solution was left for crystallization which led to the formation of crystals of **Cu-4**.

7.4 Source of 3D-$K_{6.56}Cu_{0.43}H_{2.20}[(Cu_3Cl)(K_{2.68}Cu_{0.38}(H_2O)_3(B\text{-}\alpha\text{-}BiW_9O_{33})_2]\cdot 13H_2O$ (Cu-5).

A solution of $CuSO_4\cdot 5H_2O$ (0.40 g, 1.60 mmol, 4.0 eq.) was prepared in demineralized H_2O (5 mL), the pH of this solution was 3.9. The precursor $Na_9[BiW_9O_{33}]\cdot 19.5\ H_2O$ (1.00 g, 0.41 mmol, 1.0 eq.) was added as a solid in small portions at room temperature. The volume of the reaction mixture was increased to 10 mL by adding H_2O. The reaction mixture was stirred for 2 h, and a solid precipitate was removed by filtration through celite. The pH of the reaction mixture after stirring was 5.0. A saturated solution of KCl (2 mL) was added and the reaction mixture was left

for crystallization. Yellow crystals and a fine white precipitate formed overnight. The crystals were removed carefully from the reaction mixture (41.7 mg, 3.49 %). Elemental analysis: calc. for $Bi_2ClCu_{3.81}H_{28.2}K_{9.18}O_{82}W_{18}$ (found): Bi 7.33 (7.68), Cl 0.62 (0.42), Cu 4.24 (4.29), W 58.01 (55.4), K 6.29 (6.12). (ATR FT-IR cm^{-1}): 1624, 1605, 935, 874, 837, 692, 496, 430.

7.5 Source of 1D-$Na_4K_4Cu[H_2W_{12}O_{42}]\cdot 24H_2O$ (Cu-6).

A solution of $Na_9[BiW_9O_{33}]\cdot 19.5\ H_2O$ (3.00 g, 1.24 mmol, 1.0 eq.) was prepared in demineralized H_2O (30 mL); all undissolved solids were removed by filtration. A solution of $CuSO_4\cdot 5H_2O$ (10 mL, 0.12 M) was added dropwise at room temperature and the color of the reaction mixture changed to green. A solid which precipitated during the addition was removed by filtration over celite. A saturated solution of KCl (0.75 mL) was added and the reaction mixture was left for crystallization. Colorless block-like crystals were observed in the reaction mixture after a few days.

7.6 Instrumentation

ATR FT-IR spectra were recorded with a Bruker VORTEX 70 spectrometer and a platinum ATR accessory with diamond cell. Elemental analyses were carried out by Mikroanalytisches Labor Pascher, Remagen, Germany. Powder X-ray diffraction (XRD) patterns were recorded on a STOE STADI P diffractometer in transmission mode (flat sample holders, Ge-monochromator and Cu $K_{\alpha 1}$ radiation) using a position sensitive detector (Mythen K, DECTRIS). H_2 evolution was monitored with a hydrogen sensitive Clark-type sensor (H2-NP) from Unisense. Prior to each measurement the sensor was calibrated with a two point calibration using a reference sample with a known concentration of H_2. Quantification of evolved H_2 gas was obtained from headspace samples which were analyzed by gas chromatography (Varian CP 3800 Gas Chromatograph). Photographs of crystals have been made on a Leica M10 Wild stereomicroscope, equipped with a digital photocamera. Magnetization measurements were conducted on a 7 T Quantum Design MPMS XL SQUID at a magnetic field of 1.0 T in the temperature range 2−200 K in both zero field and field cooling modes. The mass susceptibility was calculated according to $\chi = M/(H\cdot m)$ (M: magnetization, H: field strength, m: sample mass).

8 References

(1) Kortz, U.; Al-Kassem, N. K.; Savelieff, M. G.; Al Kadi, N. A.; Sadakane, M. Synthesis and Characterization of Copper-, Zinc-, Manganese-, and Cobalt-Substituted Dimeric Heteropolyanions, $[(\alpha\text{-}XW_9O_{33})_2M_3(H_2O)^3]^{n-}$ (n = 12, X = As^{III}, Sb^{III}, M = Cu^{2+}, Zn^{2+}; n = 10, X = Se^{IV}, Te^{IV}, M = Cu^{2+}) and $[(\alpha\text{-}AsW_9O_{33})_2WO(H_2O)M_2(H_2O)_2]^{10-}$ (M = Zn^{2+}, Mn^{2+}, Co^{2+}). *Inorg. Chem.* **2001**, *40*, 4742–4749.

(2) Rusu, D.; Tomasa, A. R.; Turdean, G. L.; Cojocaru, I.; Oana, B.; Rusu, M. Synthesis and investigation of the copper(II)-substituted polyoxotungstate based on α-B-$[BiW_9O_{33}]^{9-}$ units. *Rev. Roum. Chim.* **2012**, *57*, 327–336.

(3) Xu, X.; Zhang, L.; Zhang, Y.; Qi, B.; Fang, L. Synthesis and Crystal Structure of a Sandwich-type Transition Metal Complex with Tungstobismutate and Triethanolamine. *Z. Naturforsch. B.* **2009**, *64*, 821–825.

(4) Roşu, C.; Rasu, D.; Weakley, T. J. R. X-ray structure of dodecasodium tricopper(II)bis[nonatungstabismuthate(III) hydrate, a polyoxometalate salt containing α-B-BiW_9O_{33} units. *J. Chem. Crystallogr.* **2003**, *33*, 751–755.

(5) Rusu, D.; Roşu, C.; Crăciun, C.; David, L.; Rusu, M.; Marcu, G. FT-IR, UV–VIS and EPR investigations of multicopper polyoxotungstates with Bi^{III} as heteroatom. *J. Mol. Struct.* **2001**, *563–564*, 427–433.

(6) Xue, G.-L.; Wang, H.-L.; Xie, Z.-H.; Shi, Q.-Z.; Wang, J.-W.; Wang, D.-Q. Synthesis, Crystal Structure and Magnetic Property of Sandwich-Type Heteropolyoxometalate $Na_9[(Na(H_2O)_3Cu(H_2O)_3(BiW_9O_{33})_2]\cdot 42H_2O$. *Chinese J. Chem.* **2004**, *22*, 159–161.

(7) Roşu, C.; Rusu, M.; Casañ-Pastor, N.; Gómez-Garciac, C. J. Synthesis, Characterization and Electrochemistry of Cobalt(II) and Copper(II) Complexes of Bismutho(III)Polyoxotungstate Ligand Anion. *Syn. React. Inorg. Met.* **2000**, *30*, 369–377.

(8) Li, Y.-W.; Wang, Y.-H.; Li, Y.-G.; Wang, E.-B.; Chen, W.-L.; Wu, Q.; Shi, Q. A new (8,3)-connected anionic 3-D open-framework based on paradodecatungstate and Cu(II) linkers. *Inorg. Chim. Acta.* **2009**, *362*, 1078–1082.

(9) Kong, Q.-J.; Zhang, C.-J.; Chen, Y.-G. Synthesis, structure and characterization of three highly-connected 3D inorganic compounds based on paradodecatungstate-B. *J. Mol. Struct.* **2010**, *964*, 82–87.

(10) Zhang, Z. Two Novel Purely Inorganic Coordination Polymers Constructed From Bivalent Transition Metal Ions and Paratungstate Clusters. *J. Chem. Crystallogr.* **2012**, *42*, 333–337.

(11) Li, B.; Bi, L.; Li, W.; Wu, L. Synthesis, crystal structure, and property of one- and two-dimensional complexes based on paradodecatungstate-B cluster. *J. Solid State Chem.* **2008**, *181*, 3337–3343.

(12) Zhang, C.-J.; Chen, Y.-G.; Shi, D.-M.; Pang, H.-J. Synthesis and Characterization of a Three-dimensional Porous Compound: $[Cu(H_2O)_6][\{Cu(H_2O)_2\}_2\{Cu(H_2O)_4H_4W_{12}O_{42}\}] \cdot 12H_2O$. *Z. Naturforsch. B.* **2014**, *63b*, 187–192.

(13) Xu, X.; Luo, F.; Luo, W.; Chen, J. Synthesis and Crystal Structure of a New 3D Copper B-Paradodecatungstate Compound: $[Na_2(H_2O)_8][Na_8(H_2O)_{20}][Cu(en)_2][W_{12}O_{42}] \cdot 3H_2O$. *Z. Naturforsch. B.* **2009**, *64*, 269–273.

(14) Radio, S. V.; Melnik, N. A.; Ivantsova, E. S.; Baumer, V. N. Crystal structure of double sodium-copper(II) paratungstate B: $Na_2Cu_3(CuOH)_2[W_{12}O_{40}(OH)_2]\cdot 32H_2O$. *J. Struct. Chem.* **2014**, *55*, 879–886.

(15) Sun, C.-Y.; Liu, S.-X.; Wang, C.-L.; Xie, L.-H.; Zhang, C.-D.; Gao, B.; Wang, E.-B. Reactions of trivacant lone-pair-containing tungstobismutate and electrochemical behaviors of its sandwich-type products. *J. Coord. Chem.* **2007**, *60*, 567–579.

(16) Wang, B.; Hou, G.-F.; Meng, R.-Q.; Bi, L.-H.; Li, B.; Wu, L.-X. A novel NbO-type framework constructed from Dawson-like tungstobismuthate and copper complex fragments. *CrystEngComm* **2011**, *13*, 1360–1365.
(17) Sheldrick, G. M. Crystal structure refinement with SHELX. *Acta Crystallogr. C.* **2015**, *71*, 3–8.
(18) Spek, A. L. PLATON SQUEEZE: a tool for the calculation of the disordered solvent contribution to the calculated structure factors. *Acta Crystallogr. C.* **2015**, *71*, 9–18.
(19) Allen, F. H.; Johnson, O.; Shields, G. P.; Smith, B. R.; Towler, M. CIF applications. XV. enCIFer: a program for viewing, editing and visualizing CIFs. *J. Appl. Cryst.* **2004**, *37*, 335–338.
(20) Delina Barats-Damatov; Shimon, L. J. W.; Feldman, Y.; Tatyana Bendikov; Neumann, R. Solid-State Crystal-to-Crystal Phase Transitions and Reversible Structure–Temperature Behavior of Phosphovanadomolybdic Acid, $H_5PV_2Mo_{10}O_{40}$. *Inorg. Chem.* **2015**, *54*, 628–634.
(21) Winter, R. S.; De-Liang, L.; Cronin, L. Synthesis and Characterization of a Series of $[M_2(\beta\text{-}SiW_8O_{31})_2]^{n-}$ Clusters and Mechanistic Insight into the Reorganization of $\beta\text{-}SiW_8O_{31}$ into $\alpha\text{-}SiW_9O_{34}$. *Inorg. Chem.* **2015**, *54*, 4151–4155.
(22) Wang, K.-Y.; Lin, Z.; Bassil, B. S.; Xing, X.; Haider, A.; Keita, B.; Zhang, G.; Silvestru, C.; Kortz, U. Ti2-Containing 18-Tungsto-2-Arsenate(III) Monolacunary Host and the Incorporation of a Phenylantimony(III) Guest. *Inorg. Chem.* **2015**, *54*, 10530–10532.
(23) Brown, I. D.; Altermatt, D. Bond-valence parameters obtained from a systematic analysis of the Inorganic Crystal Structure Database. *Acta Crystallogr. B.* **1985**, *41*, 244–247.
(24) Choi, K.-Y.; Matsuda, Y. H.; Nojiri, H.; Kortz, U.; Hussain, F.; Stowe, A. C.; Ramsey, C.; Dalal, N. S. Observation of a Half Step Magnetization in the $\{Cu_3\}$-Type Triangular Spin Ring. *Phys. Rev. Lett.* **2006**, *96*, 107202.
(25) Kortz, U.; Nellutla, S.; Stowe, A. C.; Dalal, N. S.; van Tol, J.; Bassil, B. S. Structure and Magnetism of the Tetra-Copper(II)-Substituted Heteropolyanion $[Cu_4K_2(H_2O)_8(AsW_9O_{33})_2]^{8-}$. *Inorg. Chem.* **2004**, *43*, 144–154.
(26) Seery, M. K.; Guerin, L.; Forster, R. J.; Gicquel, E.; Hultgren, V.; Bond, A. M.; Wedd, A. G.; Keyes, T. E. Photophysics of Ion Clusters Formed between $[Ru(bpy)_3]^{2+}$ and the Polyoxotungstate Anion $[S_2W_{18}O_{62}]^{4-}$. *J. Phys. Chem. A* **2004**, *108*, 7399–7405.
(27) Keyes, T. E.; Gicquel, E.; Guerin, L.; Forster, R. J.; Hultgren, V. M.; Bond, A. M.; Wedd, A. G. Photophysical and Novel Charge-Transfer Properties of Adducts between $[Ru^{II}(bpy)_3]^{2+}$ and $[S_2Mo_{18}O_{62}]^{4-}$. *Inorg. Chem.* **2003**, *42*, 7897–7905.
(28) Gao, J.; Cao, S.; Tay, Q.; Liu, Y.; Yu, L.; Ye, K.; Mun, P. C. S.; Li, Y.; Rakesh, G.; Loo, S. C. J.; Chen, Z.; Zhao, Y.; Xue, C.; Zhang, Q. Molecule-Based Water-Oxidation Catalysts (WOCs): Cluster-Size-Dependent Dye-Sensitized Polyoxometalates for Visible-Light-Driven O_2 Evolution. *Sci. Rep.* **2013**, *3*, 1853–1858.
(29) Fay, N.; Hultgren, V. M.; Wedd, A. G.; Keyes, T. E.; Forster, R. J.; Leane, D.; Bond, A. M. Sensitization of photo-reduction of the polyoxometalate anions $[S_2M_{18}O_{62}]^{4-}$ (M = Mo, W) in the visible spectral region by the $[Ru(bpy)_3]^{2+}$ cation. *Dalton Trans.* **2006**, 4218–4227.
(30) Car, P.-E.; Guttentag, M.; Baldridge, K. K.; Alberto, R.; Patzke, G. R. Synthesis and characterization of open and sandwich-type polyoxometalates reveals visible-light-driven water oxidation via POM-photosensitizer complexes. *Green. Chem.* **2012**, *14*, 1680–1688.
(31) Stracke, J. J.; Finke, R. G. Distinguishing Homogeneous from Heterogeneous Water Oxidation Catalysis when Beginning with Polyoxometalates. *ACS Catal.* **2014**, *4*, 909–933.

(32) von Allmen, K.; Moré, R.; Müller, R.; Soriano-López, J.; Linden, A.; Patzke, G. R. Nickel-Containing Keggin-Type Polyoxometalates as Hydrogen Evolution Catalysts: Photochemical Structure–Activity Relationships. *ChemPlusChem* **2015**, *80*, 1389–1398.
(33) Bachmann, C.; Probst, B.; Guttentag, M.; Alberto, R. Ascorbate as an electron relay between an irreversible electron donor and Ru(II) or Re(I) photosensitizers. *Chem. Commun.* **2014**, *50*, 6737–6739.
(34) Evans, H. T. J.; Prince, E. Location of internal hydrogen atoms in the paradodecatungstate polyanion by neutron diffraction. *J. Am. Chem. Soc.* **1983**, *105*, 4838–4839.
(35) Botar, B.; Yamase, T.; Ishikawa, E. A highly nuclear vanadium-containing tungstobismutate: synthesis and crystal structure of $K_{11}H[(BiW_9O_{33})_3Bi_6(OH)_3(H_2O)_3V_4O_{10}]\cdot 25.5H_2O$. *Inorg. Chem. Commun.* **2000**, *3*, 579–584.